

Can't Touch This: Real-Time, Safe Motion Planning and Control for Manipulators Under Uncertainty

Jonathan Michaux¹, Patrick Holmes¹, Bohao Zhang¹, Che Chen¹, Baiyue Wang¹, Shrey Sahgal¹, Tiancheng Zhang¹, Sidhartha Dey⁴, Shreyas Kousik², and Ram Vasudevan^{1,3}

Abstract—Ensuring safe, real-time motion planning in arbitrary environments requires a robotic manipulator to avoid collisions, obey joint limits, and account for uncertainties in the mass and inertia of objects and the robot itself. This paper proposes **Autonomous Robust Manipulation via Optimization with Uncertainty-aware Reachability (ARMOUR)**, a provably-safe, receding-horizon trajectory planner and tracking controller framework for robotic manipulators to address these challenges. ARMOUR first constructs a robust controller that tracks desired trajectories with bounded error despite uncertain dynamics. ARMOUR then uses a novel recursive Newton-Euler method to compute all inputs required to track any trajectory within a continuum of desired trajectories. Finally, ARMOUR over-approximates the swept volume of the manipulator; this enables one to formulate an optimization problem that can be solved in real-time to synthesize provably-safe motions. This paper compares ARMOUR to state of the art methods on a set of challenging manipulation examples in simulation and demonstrates its ability to ensure safety on real hardware in the presence of model uncertainty without sacrificing performance. Project page: <https://roahmlab.github.io/armour/>.

I. INTRODUCTION

Robotic manipulators have the potential to assist humans in a wide variety of collaborative settings, such as manufacturing, package delivery, and in-home care. However, such settings are typically constrained and uncertain; nevertheless, the robot must operate in a safety-critical fashion. This makes it challenging to directly apply high-torque manipulators that ignore model uncertainty. Instead, it is necessary to develop motion planning and control strategies that can operate safely by accounting for these types of uncertainty in real-time. In this context, safety means avoiding collisions while obeying joint position, velocity, and torque limits. To address the safety challenge, this paper proposes **Autonomous Robust Manipulation via Optimization with Uncertainty-aware Reachability (ARMOUR)**, a method for guaranteed-safe, real-time manipulator motion planning and control. An overview of this method is given in Fig. 1. The work enables safety for uncertain manipulator dynamics, which includes

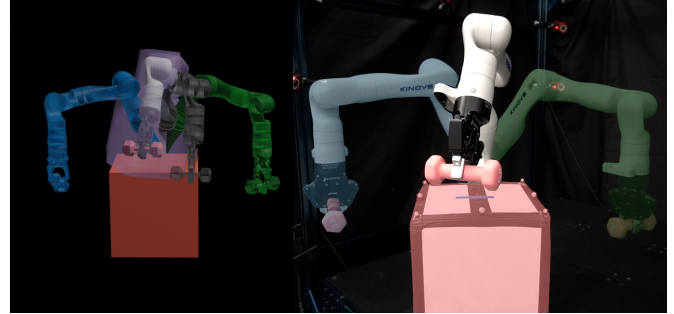


Fig. 1. This paper considers the problem of safe motion planning with uncertain dynamics; for example, when manipulating a heavy dumbbell (pink) with uncertain mass in clutter (red obstacles). ARMOUR operates in a receding horizon way, moving from the start (right panel, blue) arm to the goal (right panel, green arm) by repeatedly generating new trajectory plans in real time. In each planning iteration, ARMOUR first computes a Forward Reachable Set (FRS) for a continuum of possible motion plans (left panel, purple volume), representing the swept volume of the arm under uncertain dynamics. Many of these motion plans may be in collision, so ARMOUR solves a constrained trajectory optimization problem to find a collision-free plan that makes progress towards an intermediate waypoint (left panel, black arm) and the global goal (right panel, green arm).

uncertain payloads, by proposing a combined planning and control framework.

The focus of this paper is manipulator planning and control under uncertainty in a robot's dynamic model. Typically, one relies on an accurate model of the robot that is assumed to be true. However, it is challenging to construct a perfect model. For example, the dynamics of a robotic arm depend on inertial properties that may not be known perfectly well (e.g., link masses, center of mass locations, and inertia matrices). Similarly, a manipulator may not have access to an object's true inertial properties when grasping and transporting it. This work seeks to robustly account for set-based uncertainty in manipulator and object inertial properties.

Safety is a critical property for deploying manipulators in real-world scenarios, as collisions with people or objects (i.e., obstacles) could cause grave harm. Planning and control for collision avoidance is challenging because most obstacle-avoidance constraints are non-convex, and manipulators typically have nonlinear dynamics. This challenge is compounded by the need to obey position, velocity, and torque constraints at each joint to avoid damaging the robot. Furthermore, it is necessary to guarantee safety in continuous time, to ensure no safety violations between discrete time steps. This work ensures safety by making continuous-time guarantees on collision avoidance, actuator limits, joint position limits, and joint velocity limits. Because mobile robots must update their maps of the world as they move and collect new information,

This work is supported by the Ford Motor Company via the Ford-UM Alliance under award N022977, National Science Foundation Career Award #1751093, and by the Office of Naval Research under Award Number N00014-18-1-2575

¹Robotics Institute, University of Michigan, Ann Arbor, MI (jmichaux, pdholmes, jimzhang, ramv, cctom, baiyuew, shreyeps, zhangtc)@umich.edu.

²Mechanical Engineering, Georgia Institute of Technology, Atlanta, GA shreyas.kousik@me.gatech.edu.

³Mechanical Engineering, University of Michigan, Ann Arbor, MI ramv@umich.edu.

⁴Agility Robotics, Albany, OR sid.dey@agilityrobotics.com.

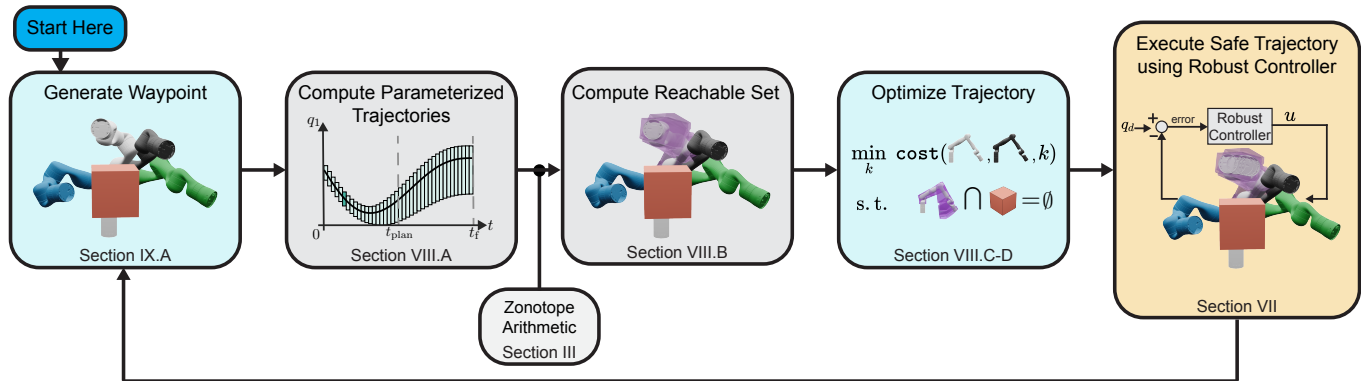


Fig. 2. Overview of ARMOUR, a receding-horizon planning and control framework for robot manipulators with uncertain dynamics. First, a high-level planner generates waypoints between the robot’s initial and goal states. Second, ARMOUR represents the time horizon as a finite set of polynomial zonotopes (Sec. VIII-A1) and computes a family of desired trajectories that are overapproximated by a finite set of polynomial zonotopes (Sec. VIII-A2). Third, ARMOUR computes the forward occupancy of the robot over this entire set (Sec. VIII-B). Fourth, ARMOUR generates safety constraints (Sec. VIII-C3) and performs optimization over the family of parameterized desired trajectories of each joint (Sec. VIII-D). Note that torque constraints and obstacle collision-avoidance constraints guarantee the safety of our method. Finally, to ensure that these trajectories can be safely followed, ARMOUR implements a robust passivity-based controller that uniformly bounds the tracking performance despite uncertainty in the robot’s dynamics (Sec. VII).

this work focuses on the development of a real-time, receding horizon planning and control method.

Contribution: To the best of our knowledge, no motion planning and control framework exists that guarantees the continuous time safety of a manipulator robot with set-based uncertainty and operates in real-time. Our framework guarantees continuous time collision avoidance and satisfaction of a robot’s torque bounds and joint limits while explicitly accounting for tracking error caused by uncertainty in the robot’s dynamics. We make the following contributions: First, we propose a novel robust passivity-based controller to safely account for uncertain robot dynamics by providing explicit tracking error guarantees. Second, we construct a novel variation of the modified Recursive Newton-Euler Algorithm (RNEA) [1], which we call polynomial zonotope RNEA (PZRNEA). This approach uses polynomial zonotopes [2] to compute sets of possible inputs required to track trajectories, and allows us to satisfy torque limit constraints during motion planning. Third, we use polynomial zonotopes to represent the forward occupancy of the robot, which is used to guarantee obstacle avoidance. Each of these contributions is used to formulate the motion planning and control problem as an optimization problem that can be tractably solved in real-time with formal safety guarantees in a receding horizon fashion. In particular, we demonstrate how to differentiate these polynomial zonotope-based representations to perform real-time optimization while providing safety guarantees. We demonstrate our method in simulation and hardware and compare it to state of the art alternatives. These experiments confirm that our method enables safe manipulation of grasped objects with uncertain inertial parameters, while other methods may cause collisions or require motions that are not realizable.

Relationship to Prior Work: ARMOUR builds upon prior work entitled Autonomous, Reachability-based Manipulator Trajectory Design (ARMTD) [3]. The prior work develops a planning algorithm for deterministic kinematic manipulator models. In contrast, this work is able to account for model uncertainty while using a dynamic model of the manipulator.

As we show in this paper, ARMOUR significantly reduces the conservativeness of ARMTD’s numerical reachable set. Lastly, ARMOUR describes a strategy for control design and is able to account for input constraints.

Method and Paper Overview: An overview of the different components of ARMOUR is illustrated in Fig. 2. The remainder of this paper is organized as follows: First, we review related work in Sec. II. Next, relevant notation and mathematical objects are introduced in Sec. III, and the robot’s kinematics, dynamics and environment are discussed in Sec. IV. Our motion planning and control hierarchy operates in a receding-horizon fashion, and is divided into a trajectory planner and a low-level robust controller. The trajectory planner performs optimization over a family of parameterized desired trajectories of each joint (Sec. VI). To ensure that these trajectories can be safely followed we implement a robust passivity-based controller that uniformly bounds the tracking performance despite uncertainty in the robot’s dynamics (Sec. VII). Online, the desired trajectories buffered by this uniform bound are assembled into reachable sets of the full arm to bound the robot’s motion through the workspace and utilized within PZRNEA to bound the inputs required to track any desired trajectory (Sec. VIII). Torque constraints and obstacle collision-avoidance constraints guarantee the safety of our method within an online trajectory optimization program, which generates a desired trajectory to be tracked by the robust controller. We then demonstrate the efficacy of our method for safely manipulating uncertain grasped objects in simulation and in the real-world, and we compare it to other state of the art methods (Sec. IX).

II. BACKGROUND AND RELATED WORK

This paper addresses the problem of real-time, safe manipulation planning and control that accounts for uncertain dynamics. A common approach to solving similar problems is to use a global, sampling-based path planner to generate coarse, high-level motions, then a local planner to generate

trajectories, and finally a controller to track the trajectories (e.g., [4], [5], and our own prior work [3], [6]).

It is challenging to generate motion plans to complete tasks while obeying constraints in real time due to the high-dimensional models used to describe manipulators. Planning methods can be categorized depending upon how physics are represented: one can ignore physics (i.e., path or kinematic planning), or represent dynamics. Methods can also be categorized by how plans are synthesized, using either sampling [7], [8] or optimization [9], [10]. Note, further categorization can be applied depending upon how the robot and its environment are represented [11], [12]. Recall that the present work considers real-time, optimization-based motion planning for manipulators with uncertain dynamics. To proceed, we review how kinematics, dynamics, and uncertainty have been considered in sampling- and optimization-based approaches; note that a thorough survey is available [12].

A common approach to enable fast performance is to plan a path or a kinematic trajectory, then rely on an underlying feedback controller to compensate for the robot’s true dynamics. Our previous work [3] employed this strategy, as do a variety of optimization-based planners [9], [10], [13]. This approach is also used in sampling-based motion planning for complex robots such as manipulators or humanoids, often by directly modeling the configuration manifold [14], [15], though these approaches are not typically fast enough for real time replanning. To increase computational efficiency, one can instead precompute some constraint manifolds [16]. With these methods, computational speed comes at the expense of not modeling the dynamics of the robot.

An alternate approach is to incorporate a model of the robot’s dynamics during planning. Notably, researchers have extended the well-known Rapidly-exploring Random Trees (RRT) algorithm [17] to incorporate torque and friction constraints in discrete time by projection to constraint manifolds [18], though this approach cannot plan in real time. More recently, it has been shown how to verify robot motion near humans by rapidly computing capsule-shaped safety zones for manipulator dynamics [19]–[21]; however, these methods do not account for uncertainty in the dynamics. These previous methods focus on collision avoidance for manipulators; however, we note that there is extensive work on humanoid motion planning with dynamics, typically by planning a sequence of static, dynamically-feasible poses [22]–[24]. These latter methods do not operate in real time due to the high-dimensional nature of humanoid robots. Altogether, it remains a challenge to rapidly plan collision-free manipulator motion while incorporating uncertain dynamics.

As mentioned above, to achieve fast performance, most approaches plan kinematic paths or trajectories, then rely on a lower-level controller to obey dynamic constraints. We briefly note that some approaches instead merge kinematic planning and control [25], [26] by generalizing the notion of potential fields. While these methods can guarantee kinematic collision avoidance in discrete time [26], they do not incorporate dynamics. There is a long history of constructing control strategies to account for manipulator dynamics [27], [28]. The core challenge is to develop a controller that guarantees con-

vergence to a given desired trajectory despite disturbance and uncertain, nonlinear dynamics. A further challenge is to ensure these controllers are continuous, to avoid chattering or exciting high-frequency dynamics that are not typically modeled [29], [30]. To handle parametric uncertainty, a variety of adaptive and sliding-mode control approaches have been proposed that prove both convergence and bounds on trajectory tracking error by simultaneously controlling a robot and estimating its uncertain parameters [31]–[34].

One of the key challenges with such techniques is to estimate bounds on the nonlinear perturbations to the controlled system [32]. A recent alternative has been to directly compute the reachable set of states for a manipulator with parameter uncertainty via interval arithmetic for verification [35]–[37] while building off of existing techniques for linear systems [38], [39] and nonlinear systems [40], [41]. The present work develops a novel controller that improves on previous interval arithmetic-based methods in three ways. First, our controller generates smaller inputs that achieve the same tracking error performance. Second, this allows us to build tighter tracking error bounds in practice (see [online appendix](#)). Third, we demonstrate that our controller is not only useful for verification, but also planning.

III. PRELIMINARIES

To describe the swept volume of a manipulator subject to uncertain dynamics, we leverage two numerical set representations: intervals and polynomial zonotopes. This section describes our notation conventions and each set representation.

A. Notation

The n -dimensional real numbers are \mathbb{R}^n , natural numbers \mathbb{N} , the unit circle is \mathbb{S}^1 , and the set of 3×3 orthonormal matrices is $\text{SO}(3)$. Subscripts may index elements of a vector or a set, or provide additional context. For a matrix A , we use A^\top to denote its transpose. We use the product notation $\prod_{i=1}^m A_i = A_1 A_2 \cdots A_m$ to denote successive matrix multiplications, where $A_i \in \mathbb{R}^{n \times n}$. Vector concatenation is denoted (x_1, \dots, x_n) unless the shape is critical to understanding, in which case we write $[x_1^\top, \dots, x_n^\top]^\top$.

Let $U, V \subset \mathbb{R}^n$. For a point $u \in U$, $\{u\} \subset U$ is the set containing only u . The *power set* of U is $\text{pow}(U)$. The *Minkowski Sum* is $U \oplus V = \{u + v \mid u \in U, v \in V\}$; the *Minkowski Difference* is $U \ominus V = U \oplus (-V)$. For vectors $a, b \in \mathbb{R}^3$, we write the cross product as $a \times b$, where

$$a \times b = \begin{bmatrix} 0 & -a_3 & a_2 \\ a_3 & 0 & -a_1 \\ -a_2 & a_1 & 0 \end{bmatrix}. \quad (1)$$

If $n = 3$, the *set-based cross product* is defined as $U \otimes V = \{u \times v \mid u \in U, v \in V\}$. If $\{U_i \subset \mathbb{R}^n\}_{i=1}^m$ then let $\times_{i=1}^m U_i$ denote the Cartesian product of the U_i ’s. Let $W \subset \mathbb{R}^{n \times n}$ be a set of square matrices. Then, *set-based multiplication* is defined as $WV = \{Av, \mid A \in W, v \in V\}$. Let 0 (resp. 1) denote a matrix of zeros (resp. ones) of appropriate size, and let I_n be the $n \times n$ identity matrix.

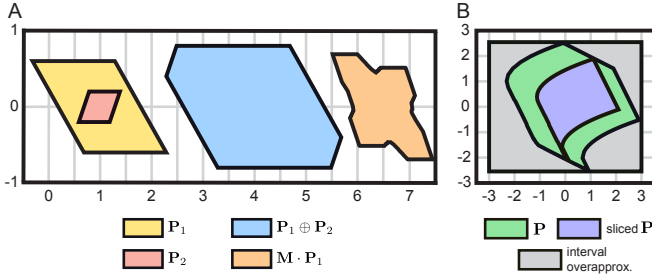


Fig. 3. Illustration of polynomial zonotope arithmetic. (A) The middle panel shows the minkowski sum (blue) of polynomial zonotopes \mathbf{P}_1 (gold) and \mathbf{P}_2 (red). The right panel shows the multiplication (orange) of \mathbf{P}_1 by a matrix M . (B) A polynomial zonotope \mathbf{P} , shown in green, is sliced to produce the polynomial zonotope shown in purple. The grey rectangle represents an interval overapproximation of \mathbf{P} .

B. Intervals

We describe uncertain manipulator parameters as intervals (see [42], [43] for an overview of interval arithmetic). An n -dimensional interval is a set

$$[x] = \{y \in \mathbb{R}^n \mid x_i \leq y_i \leq \bar{x}_i, \forall i = 1, \dots, n\}. \quad (2)$$

When the bounds are important, we denote an interval $[x]$ by $[\underline{x}, \bar{x}]$, where \underline{x} and \bar{x} are the infimum and supremum, respectively, of $[x]$. Let $\inf([x]) := \underline{x}$ and $\sup([x]) := \bar{x}$. Let $\mathbb{I}\mathbb{R}^n$ be the set of all real-valued n -dimensional interval vectors. The Minkowski sum and difference of $[x]$ and $[y]$ are

$$[x] \oplus [y] = [\underline{x} + \underline{y}, \bar{x} + \bar{y}], \quad (3)$$

$$[x] \ominus [y] = [\underline{x} - \bar{y}, \bar{x} - \underline{y}]. \quad (4)$$

The product of $[x]$ and $[y]$ is

$$[x][y] = [\min(\underline{x}\underline{y}, \underline{x}\bar{y}, \bar{x}\underline{y}, \bar{x}\bar{y}), \max(\underline{x}\underline{y}, \underline{x}\bar{y}, \bar{x}\underline{y}, \bar{x}\bar{y})]. \quad (5)$$

The i^{th} and j^{th} entry of the product of an interval matrix $[Y]$ multiplied by an interval matrix $[X]$ is

$$([X][Y])_{ij} = \bigoplus_{k=1}^n ([X]_{ik}[Y]_{kj}), \quad (6)$$

where n is the number of columns of $[X]$ and number of rows of $[Y]$. Given interval vectors $[x], [y] \subset \mathbb{R}^3$, their cross product is

$$[x] \otimes [y] = [x]^\times [y], \quad (7)$$

where $[x]^\times$ is the skew-symmetric matrix representation of $[x]$ as in (1) (i.e., a matrix with interval entries).

C. Polynomial Zonotopes

We present an overview of the necessary definitions and operations of polynomial zonotopes (PZs) in this subsection. A thorough introduction is available [2] and illustration of the operations we perform on PZs can be found in Fig. 3.

Given generators $g_i \in \mathbb{R}^n$ and exponents $\alpha_i \in \mathbb{N}_{n_g}$ for $i \in \{0, \dots, n_g\}$, a polynomial zonotope is a set:

$$\mathbf{P} = \mathcal{PZ}(g_i, \alpha_i, x) = \{z \in \mathbb{R}^n \mid z = \sum_{i=0}^{n_g} g_i x^{\alpha_i}, x \in [-1, 1]^{n_g}\}. \quad (8)$$

In this paper, we set the exponent associated with the zeroth generator to be zero, i.e., $\alpha_0 = [0, 0, \dots, 0]$. We refer to x^{α_i} as a *monomial*, $x \in [-1, 1]^{n_g}$ as *indeterminates*, and g_0 as the *center*. A term $g_i x^{\alpha_i}$ is produced by multiplying a monomial by the associated generator g_i . Throughout this document, we exclusively use bold symbols to denote polynomial zonotopes.

Next, we introduce several useful operations on polynomial zonotopes: interval conversions, set addition and multiplication, slicing, computing bounds, and set-valued function evaluation. Table I summarizes these operations. Importantly, these operations can either be computed exactly or in an overapproximative fashion using polynomial zonotopes.

1) *Intervals Conversion*: Intervals can also be written as polynomial zonotopes. For example, let $[z] = [\underline{z}, \bar{z}] \subset \mathbb{R}^n$, then one can convert $[z]$ to a polynomial zonotope \mathbf{z} using

$$\mathbf{z} = \frac{\bar{z} + \underline{z}}{2} + \sum_{i=1}^n \frac{\bar{z}_i - \underline{z}_i}{2} x_i, \quad (9)$$

where $x \in [-1, 1]^n$ is the indeterminate vector.

2) *Set Addition and Multiplication*: The Minkowski Sum of two polynomial zonotopes $\mathbf{P}_1 \subset \mathbb{R}^n = \mathcal{PZ}(g_i, \alpha_i, x)$ and $\mathbf{P}_2 \subset \mathbb{R}^n = \mathcal{PZ}(h_j, \beta_j, y)$ follows from polynomial addition:

$$\mathbf{P}_1 \oplus \mathbf{P}_2 = \left\{ z \in \mathbb{R}^n \mid z = \sum_{i=0}^{n_g} g_i x^{\alpha_i} + \sum_{j=0}^{n_h} h_j y^{\beta_j} \right\}. \quad (10)$$

Similarly, we may write the matrix product of two polynomial zonotopes \mathbf{P}_1 and \mathbf{P}_2 when the sizes are compatible. Letting $\mathbf{P}_1 \subset \mathbb{R}^{n \times m}$ and $\mathbf{P}_2 \subset \mathbb{R}^{m \times k}$, we obtain $\mathbf{P}_1 \mathbf{P}_2 \subset \mathbb{R}^{n \times k}$:

$$\mathbf{P}_1 \mathbf{P}_2 = \left\{ z \in \mathbb{R}^{n \times k} \mid z = \sum_{i=0}^{n_g} g_i \left(\sum_{j=0}^q h_j y^{\beta_j} \right) x^{\alpha_i} \right\}. \quad (11)$$

When $\mathbf{P}_1 \subset \mathbb{R}^{n \times n}$ is square, exponentiation \mathbf{P}_1^m may be performed by multiplying \mathbf{P}_1 by itself m times. Furthermore, if $\mathbf{P}_1 \subset \mathbb{R}^3$ and $\mathbf{P}_2 \subset \mathbb{R}^3$, we implement a set-based cross product as matrix multiplication. We create $\mathbf{P}_1^\times \subset \mathbb{R}^{3 \times 3}$ as

$$\mathbf{P}_1^\times = \left\{ A \in \mathbb{R}^{3 \times 3} \mid A = \sum_{i=0}^{n_g} \begin{bmatrix} 0 & -g_{i,3} & g_{i,2} \\ g_{i,3} & 0 & -g_{i,1} \\ -g_{i,2} & g_{i,1} & 0 \end{bmatrix} x^{\alpha_i} \right\} \quad (12)$$

where $g_{i,j}$ refers to the j^{th} element of g_i . Then, the set-based cross product $\mathbf{P}_1 \otimes \mathbf{P}_2 = \mathbf{P}_1^\times \mathbf{P}_2$ is well-defined.

3) *Slicing*: One can obtain subsets of polynomial zonotopes by plugging in values of known indeterminates. For instance, if a polynomial zonotope \mathbf{P} represented a set of possible positions of a robot arm operating near an obstacle. It may be beneficial to know whether a particular choice of \mathbf{P} 's indeterminates yields a subset of positions that could collide with the obstacle. To this end, "slicing" a polynomial zonotope

TABLE I
Summary of polynomial zonotope operations.

Operation	Computation
$[z] \rightarrow \mathbf{z}$ (Interval Conversion) (9)	Exact
$\mathbf{P}_1 \oplus \mathbf{P}_2$ (Minkowski Sum) (10)	Exact
$\mathbf{P}_1 \mathbf{P}_2$ (Set Multiplication) (11)	Exact
\mathbf{P}_1^m (Exponentiation)	Exact
$\mathbf{P}_1 \otimes \mathbf{P}_2$ (Set Cross Product) (12)	Exact
$\text{slice}(\mathbf{P}, x_j, \sigma)$ (13)	Exact
$\sup(\mathbf{P})$ (14) and $\inf(\mathbf{P})$ (15)	Overapproximative
$f(\mathbf{P}_1) \subseteq \mathbf{P}_2$ (Taylor expansion) (20)	Overapproximative

$\mathbf{P} = \mathcal{PZ}(g_i, \alpha_i, x)$ corresponds to evaluating an element of the indeterminate x . Given the j^{th} indeterminate x_j and a value $\sigma \in [-1, 1]$, slicing yields a subset of \mathbf{P} by plugging σ into the specified element x_j :

$$\text{slice}(\mathbf{P}, x_j, \sigma) \subset \mathbf{P} = \left\{ z \in \mathbf{P} \mid z = \sum_{i=0}^{n_g} g_i x^{\alpha_i}, x_j = \sigma \right\}. \quad (13)$$

4) *Bounding a PZ*: Our algorithm requires a means to bound the elements of a polynomial zonotope. We define the sup and inf operations which return these upper and lower bounds, respectively, by taking the absolute values of generators. For $\mathbf{P} \subseteq \mathbb{R}^n$ with center g_0 and generators g_i ,

$$\text{sup}(\mathbf{P}) = g_0 + \sum_{i=1}^{n_g} |g_i|, \quad (14)$$

$$\text{inf}(\mathbf{P}) = g_0 - \sum_{i=1}^{n_g} |g_i|. \quad (15)$$

Note that for any $z \in \mathbf{P}$, $\text{sup}(\mathbf{P}) \geq z$ and $\text{inf}(\mathbf{P}) \leq z$, where the inequalities are taken element-wise. These bounds may not be tight, but they are quick to compute.

5) *Set-Valued Function Evaluation*: One can overapproximate any analytic function evaluated on a polynomial zonotope using a Taylor expansion, which itself can be represented as a polynomial zonotope [44, Sec 4.1],[2, Prop. 13]. Consider an analytic function $f: \mathbb{R} \rightarrow \mathbb{R}$ and $\mathbf{P}_1 = \mathcal{PZ}(g_i, \alpha_i, x)$, with each $g_i \in \mathbb{R}$, then $f(\mathbf{P}_1) = \{y \in \mathbb{R} \mid y = f(z), z \in \mathbf{P}_1\}$. We generate \mathbf{P}_2 such that $f(\mathbf{P}_1) \subseteq \mathbf{P}_2$ using a Taylor expansion of degree $d \in \mathbb{N}$, where the error incurred from the finite approximation is overapproximated using a Lagrange remainder. The method follows the Taylor expansion found in the reachability algorithm in [2], which builds on previous work on conservative polynomialization found in [44]. Recall that the Taylor expansion about a point $c \in \mathbb{R}$ is

$$f(z) = \sum_{n=0}^{\infty} \frac{f^{(n)}(c)}{n!} (z-c)^n, \quad (16)$$

where $f^{(n)}$ is the n^{th} derivative of f . The error incurred by a finite Taylor expansion can be bounded using the Lagrange remainder r [45, p. 7.7]:

$$\left| f(z) - \sum_{n=0}^d \frac{f^{(n)}(c)}{n!} (z-c)^n \right| \leq r, \quad (17)$$

where

$$r = \max_{\delta \in [c, z]} \frac{(|f^{(d+1)}(\delta)|) |z-c|^{d+1}}{(d+1)!}. \quad (18)$$

For a polynomial zonotope, the infinite dimensional Taylor expansion is given by

$$f(\mathbf{P}_1) = \sum_{n=0}^{\infty} \frac{f^{(n)}(c)}{n!} (\mathbf{P}_1 - c)^n. \quad (19)$$

In practice, only a finite Taylor expansion of degree $d \in \mathbb{N}$ can be computed. Letting $c = g_0$ (i.e., the center of \mathbf{P}_1), and noting that $(z-c) = \sum_{i=1}^{n_g} g_i x^{\alpha_i}$ for $z \in \mathbf{P}_1$, we write

$$\mathbf{P}_2 := \left\{ z \in \mathbb{R} \mid z \in \sum_{n=0}^d \left(\frac{f^{(n)}(g_0)}{n!} \left(\sum_{i=1}^{n_g} g_i x^{\alpha_i} \right)^n \right) \oplus [r] \right\}, \quad (20)$$

and the Lagrange remainder $[r]$ is computed using interval arithmetic as

$$[r] = \frac{[f^{(d+1)}(\mathbf{P}_1)] [(\mathbf{P}_1 - c)^{d+1}]}{(d+1)!} \quad (21)$$

where $[(\mathbf{P}_1 - c)^{d+1}] = [\text{inf}((\mathbf{P}_1 - c)^{d+1}), \text{sup}((\mathbf{P}_1 - c)^{d+1})]$ is an overapproximation of $(\mathbf{P}_1 - c)^{d+1}$. \mathbf{P}_2 can be expressed as a polynomial zonotope because all terms in the summation are polynomials of x , and the interval $[r]$ can be expressed as a polynomial zonotope as in (9). We denote the polynomial zonotope overapproximation of a function evaluated on a zonotope using bold symbols (i.e., $\mathbf{f}(\mathbf{P}_1)$ is the polynomial zonotope overapproximation of f applied to \mathbf{P}).

IV. ARM AND ENVIRONMENT

This section introduces the robot arm's kinematics and dynamics, and defines the environment and obstacles.

A. Robotic Manipulator Model

Given an n_q -dimensional serial robotic manipulator with configuration space \mathcal{Q} and a compact time interval $T \subset \mathbb{R}$ we define a trajectory for the configuration as $q: T \rightarrow \mathcal{Q} \subset \mathbb{R}^{n_q}$. The trajectory's velocity is $\dot{q}: T \rightarrow \mathbb{R}^{n_q}$. Let $N_q = \{1, \dots, n_q\}$. We assume the following about the robot model:

Assumption 1 (Workspace and Configuration Space). *The robot operates in a three dimensional workspace, $W \subset \mathbb{R}^3$. The robot is composed of only revolute joints, where the j^{th} joint actuates the robot's j^{th} link. The robot's j^{th} joint has position and velocity limits given by $q_j(t) \in [q_{j,\text{lim}}^-, q_{j,\text{lim}}^+]$ and $\dot{q}_j(t) \in [\dot{q}_{j,\text{lim}}^-, \dot{q}_{j,\text{lim}}^+]$ for all $t \in T$, respectively. During online operation, the robot has encoders that allow it to measure its joint positions and velocities. The robot is fully actuated, where the robot's input $u: T \rightarrow \mathbb{R}^{n_q}$ has limits, i.e., $u_j(t) \in [u_{j,\text{lim}}^-, u_{j,\text{lim}}^+]$ for all $t \in T$ and $j \in N_q$.*

We make the one-joint-per-link assumption with no loss of generality because joints with multiple degrees of freedom (e.g., spherical joints) may be represented in this framework using links with zero length. In addition, this work can be extended to robots with prismatic joints by extending the RNEA algorithms presented in Sec. VIII.

1) *Arm Kinematics*: Suppose there exists a fixed inertial reference frame, which we call the *world* frame. In addition suppose there exists a *base* frame, which we denote the 0^{th} frame, that indicates the origin of the robot's kinematic chain. We assume that the j^{th} reference frame $\{\hat{x}_j, \hat{y}_j, \hat{z}_j\}$ is attached to the robot's j^{th} revolute joint, and that $\hat{z}_j = [0, 0, 1]^T$ corresponds to the j^{th} joint's axis of rotation. For a configuration at a particular time, $q(t)$, the position and orientation of frame j with respect to frame $j-1$ can be expressed using the homogeneous transformation matrix $H_j^{j-1}(q_j(t))$ [46, Ch. 2]:

$$H_j^{j-1}(q_j(t)) = \begin{bmatrix} \mathbf{R}_j^{j-1}(q_j(t)) & p_j^{j-1} \\ 0 & 1 \end{bmatrix}, \quad (22)$$

where $\mathbf{R}_j^{j-1}(q_j(t))$ is a configuration-dependent rotation matrix and p_j^{j-1} is the fixed translation vector from frame $j-1$ to

frame j . Let $\text{FK}_j : Q \rightarrow \mathbb{R}^{4 \times 4}$ map the robot's configuration to the position and orientation of the j^{th} joint in the world frame:

$$\text{FK}_j(q(t)) = \prod_{l=1}^j H_l^{l-1}(q_l(t)) = \begin{bmatrix} R_j(q(t)) & p_j(q(t)) \\ 0 & 1 \end{bmatrix}, \quad (23)$$

where

$$R_j(q(t)) := R_j^0(q(t)) = \prod_{l=1}^j R_l^{l-1}(q_l(t)), \quad (24)$$

$$p_j(q(t)) := \sum_{l=1}^j R_l(q(t)) p_l^{l-1}. \quad (25)$$

2) *Arm Occupancy*: Let $L_j \subset \mathbb{R}^3$ denote the volume occupied by the j^{th} link with respect to the j^{th} reference frame. The forward occupancy of link j is given by $\text{FO}_j : Q \rightarrow \text{pow}(W)$ defined as:

$$\text{FO}_j(q(t)) = p_j(q(t)) \oplus R_j(q(t))L_j, \quad (26)$$

where the first term gives the position of joint j and the second gives the rotated volume of link j . The volume occupied by the arm in the workspace is given by:

$$\text{FO}(q(t)) = \bigcup_{j=1}^{n_q} \text{FO}_j(q(t)). \quad (27)$$

3) *Arm Dynamics*: The robot is composed of n_q rigid links with inertial parameters:

$$\Delta = (m_1, \dots, m_{n_q}, c_{x,1}, \dots, c_{z,n_q}, I_{xx,1}, \dots, I_{zz,n_q}) \quad (28)$$

where m_j , $c_j = (c_{x,j}, c_{y,j}, c_{z,j})$, and $(I_{xx,j}, \dots, I_{zz,j})$ represent the mass, center of mass, and inertia tensor of the j^{th} link, respectively. The dynamics are represented by the standard manipulator equations [46]:

$$M(q(t), \Delta) \ddot{q}(t) + C(q(t), \dot{q}(t), \Delta) \dot{q}(t) + G(q(t), \Delta) = u(t) \quad (29)$$

where $M(q(t), \Delta) \in \mathbb{R}^{n_q \times n_q}$ is the positive definite inertia matrix, $C(q(t), \dot{q}(t), \Delta)$ is the Coriolis matrix, $G(q(t), \Delta)$ is the gravity vector, and $u(t)$ is the input torque all at time t . For simplicity, we do not explicitly model friction, but it can be incorporated in $G(q(t), \Delta)$ [35], [37]. We assume the following about the inertial parameters:

Assumption 2 (Inertial Parameter Bounds). *The model structure (i.e., number of joints, sizes of links, etc.) of the robot is known, but its true inertial parameters Δ are unknown. The uncertainty in each inertial parameter is given by*

$$[\Delta] = ([m_1], \dots, [m_{n_q}], [c_{x,1}], \dots, [c_{z,n_q}], [I_{xx,1}], \dots, [I_{zz,n_q}])^\top \quad (30)$$

where $[m_j] \subset \mathbb{R}$, $[c_j] \subset \mathbb{R}^3$, and $[I_j] \subset \mathbb{R}^{3 \times 3}$ represent the uncertainties in the mass, center of mass, and inertia tensor of the j^{th} link, respectively. The true parameters lie in this interval. Any inertia tensor drawn from $[I_j]$ must be positive semidefinite. If we let $[\Delta]_j$ denote the j^{th} component of $[\Delta]$, then $\inf([\Delta]_j) > -\infty$ and $\sup([\Delta]_j) < \infty$ for all j . There exists a nominal vector of inertial parameters $\Delta_0 \in [\Delta]$ that serves as an estimate of the true parameters of the system.

We do not assume that Δ_0 is equal to the true parameters.

B. Environment

Next, we describe obstacles and the start and goal configurations of the robot.

1) *Obstacles*: We begin by defining obstacles:

Assumption 3 (Obstacles). *The transformation between the world frame of the workspace and the base frame of the robot is known, and obstacles are expressed in the base frame of the robot. At any time, the number of obstacles $n_\mathcal{O} \in \mathbb{N}$ in the scene is finite ($n_\mathcal{O} < \infty$). Let \mathcal{O} be the set of all obstacles $\{O_1, O_2, \dots, O_{n_\mathcal{O}}\}$. Each obstacle is convex, bounded, and static with respect to time. The arm has access to a zonotope overapproximation of each obstacle's volume in workspace.*

The arm is *in collision* with an obstacle if $\text{FO}_j(q(t)) \cap O_i \neq \emptyset$ for any $j \in N_q$ or $i \in \{1, \dots, n_\mathcal{O}\}$. This work is concerned with planning and control around obstacles, not perception of obstacles. A convex, bounded object can always be overapproximated as a zonotope [47]. If one is given a non-convex bounded obstacle, then one can outerapproximate that obstacle by computing its convex hull. Dynamic obstacles may also be considered within the ARMOUR framework by introducing a more general notion of safety [48, Def. 11], but we omit this case in this paper to ease exposition. We have assumed for convenience that the robot is able to sense all obstacles workspace. One could instead assume that the robot has a finite sensing horizon in which it is able to sense obstacles. In this instance, one could extend the results regarding the collision free behavior of ARMOUR by applying Thm. 39 in [6]. If a portion of the scene is occluded, then one can treat that portion of the scene as an obstacle.

2) *Task Specification*: We define the arm's task in terms of its start and goal configurations:

Definition 4 (Start and Goal Configurations). *The robot begins from rest from the known starting configuration q_{start} . It has zero initial velocity and zero initial acceleration. ARMOUR attempts to find and execute a sequence of safe trajectories from q_{start} to a user-specified goal configuration, q_{goal} .*

If desired, an end-effector goal position in workspace may be specified instead of the configuration q_{goal} . We omit this case as it only affects ARMOUR's user-specified cost function.

V. PROPOSED METHOD OVERVIEW

This section provides a high-level overview of ARMOUR. Our objective is to plan safe trajectories in a receding horizon fashion that reach a goal configuration $q_{\text{goal}} \in Q$. To accomplish this goal, ARMOUR optimizes over a space of possible desired trajectories. As described in Sec. VI, these desired trajectories are chosen from a prespecified continuum of trajectories, with each determined by a *trajectory parameter*, $k \in K$. During each planning iteration, ARMOUR selects a trajectory parameter that can be followed without collisions despite tracking error and model uncertainty while satisfying joint and input limits. To ensure that ARMOUR is able to plan in real-time, each desired trajectory is followed while the robot constructs the next desired trajectory for the subsequent step. Next, we give overviews of the feedback controller, planning time, and trajectory optimization problem.

A. Feedback Controller

As described in Sec. VII, we associate a feedback control input over a compact time interval $T = [0, t_f] \subset \mathbb{R}$ with each trajectory parameter $k \in K$. This feedback control input is a function of the nominal inertial parameters, Δ_0 , the interval inertial parameters $[\Delta]$, and the state of the robot; however, it cannot be a function of the true inertial parameters of the robot because these are not known. Applying this control input to the arm generates an associated trajectory of the arm. This position and velocity trajectory is a function of the true inertial parameters. We denote the position and velocity trajectories at time $t \in T$ under trajectory $k \in K$ under the true inertia model parameters $\Delta \in [\Delta]$ by $q(t; k, \Delta)$ and $\dot{q}(t; k, \Delta)$, respectively. To simplify notation, *just* in this section, we denote the feedback control input at time $t \in T$ under trajectory $k \in K$ by $u(t; k)$.

Remark 5 (Controller Dependency Notation). *In the remainder of the paper, the control input is a function of the nominal inertial parameters, Δ_0 , the interval inertial parameters, $[\Delta]$, the state of the system, and the trajectory parameter.*

B. Timing

Because ARMOUR performs receding horizon planning, we assume without loss of generality that the control input and trajectory begin at time $t = 0$ and end at a fixed time t_f . To ensure real-time operation, ARMOUR identifies a new trajectory parameter within a fixed planning time of t_p seconds, where $t_p < t_f$. ARMOUR must select a new trajectory parameter before completing its tracking of the previously identified desired trajectory. If no new trajectory parameter is found in time, ARMOUR defaults to a braking maneuver that brings the robot to a stop at time $t = t_f$. As is described in Sec. VI, each desired trajectory contains a braking maneuver.

C. Online Trajectory Optimization

During each receding-horizon planning iteration, ARMOUR generates a trajectory by solving a tractable representation of the following nonlinear optimization:

$$\min_{k \in K} \text{cost}(k) \quad (31)$$

$$q_j(t; k, \Delta) \in [q_{j,\text{lim}}^-, q_{j,\text{lim}}^+] \quad \forall t \in T, \Delta \in [\Delta], j \in N_q \quad (32)$$

$$\dot{q}_j(t; k, \Delta) \in [\dot{q}_{j,\text{lim}}^-, \dot{q}_{j,\text{lim}}^+] \quad \forall t \in T, \Delta \in [\Delta], j \in N_q \quad (33)$$

$$u_j(t; k) \in [u_{j,\text{lim}}^-, u_{j,\text{lim}}^+] \quad \forall t \in T, \Delta \in [\Delta], j \in N_q \quad (34)$$

$$\text{FO}_j(q(t; k, \Delta)) \cap \emptyset = \emptyset \quad \forall t \in T, \Delta \in [\Delta], j \in N_q \quad (35)$$

The cost function (31) specifies a user-defined objective, such as bringing the robot close to some desired goal. Each of the constraints guarantee the safety of any feasible trajectory parameter as we describe next. The trajectory must be executable by the robot, which means the trajectory must not violate the robot's joint position (32), velocity (33), or input (34) limits. These constraints must be satisfied for each joint over the entire planning horizon despite model uncertainty; The robot must not collide with any obstacles in the environment (35).

Implementing a real-time algorithm to solve this problem is challenging for several reasons. First, the dynamics of the

robot are nonlinear and constructing an explicit solution to them is intractable. Second, the constraints associated with obstacle avoidance are non-convex. Finally, the constraints must be satisfied for all time $t \in T$. To address these three challenges, Sec. VIII proposes a method to generate tight overapproximations to the trajectories and constraints that are differentiable and enable the application of fast optimization techniques.

VI. TRAJECTORY DESIGN

At runtime, ARMOUR computes safe trajectories in a receding-horizon manner by solving an optimization program over parameterized trajectories at each planning iteration. This section describes the parameterized trajectories.

In each planning iteration, ARMOUR chooses a desired trajectory to be followed by the robot. These trajectories are chosen from a pre-specified continuum of trajectories, with each uniquely determined by a trajectory parameter $k \in K$. The set $K \subset \mathbb{R}^{n_k}$, $n_k \in \mathbb{N}$, is compact and represents a user-designed continuum of trajectories. K can be designed to include trajectories designed for a wide variety of tasks and robot morphologies [3], [6], [49], [50], as long as each trajectory satisfies the following definition.

Definition 6 (Trajectory Parameters). *For each $k \in K$, a desired trajectory is an analytic function $q_d(\cdot; k): T \rightarrow Q$ that satisfies the following properties:*

- I. *The trajectory starts at a specified initial condition $(q_{d_0}, \dot{q}_{d_0}, \ddot{q}_{d_0})$, so that $q_d(0; k) = q_{d_0}$, $\dot{q}_d(0; k) = \dot{q}_{d_0}$, and $\ddot{q}_d(0; k) = \ddot{q}_{d_0}$.*
- II. *$\dot{q}_d(t_f; k) = 0$ and $\ddot{q}_d(t_f; k) = 0$ (i.e., each trajectory brakes to a stop, and at the final time has zero velocity and acceleration).*
- III. *$\ddot{q}_d(\cdot; k)$ is Lipschitz continuous and bounded.*

The first property allows for desired trajectories to be generated online. In particular, recall that ARMOUR performs real-time receding horizon planning by executing a desired trajectory computed at a previous planning iteration while constructing a desired trajectory for the subsequent time interval. The first property allows desired trajectories that are generated by ARMOUR to begin from the appropriate future initial condition of the robot. The second property ensures that a fail safe braking maneuver is always available. The third property ensures that desired position, velocity, and acceleration trajectories for the tracking controller are sufficiently continuous to prove a tracking error bound as we describe next.

VII. CONTROLLER DESIGN

This section describes a robust passivity-based controller that is used to follow the desired trajectories described in the previous section. The controller conservatively handles uncertainty in the manipulator's dynamics stemming from uncertain inertial parameters, and provides a bound on the worst-case tracking error. We use this bound to develop obstacle avoidance and torque limit constraints in Sec. VIII

that are guaranteed to be satisfied when tracking a feasible desired trajectory.

The robust passivity-based controller is a feedback control input that is a function of a desired trajectory parameter. Recall that in Sec. V, we denote the control input at time $t \in T$ under trajectory $k \in K$ by $u(t; k)$ even though it is a function of the nominal inertial parameters, Δ_0 , the interval inertial parameters, $[\Delta]$, and the state of the system. Because this section focuses on proving several important properties regarding the continuity of the controller, we are deliberate in describing the controller's dependencies. Note that all desired and actual trajectories of the robot depend on the trajectory parameter $k \in K$; however, to avoid overburdening the reader, and because it is clear in context, we drop the dependence of the trajectory on k .

To formulate the controller, we define a *total feedback trajectory*, q_A , that is made up of the robot trajectory and the desired trajectory and is defined as:

$$q_A(t) = [q(t)^\top \quad \dot{q}(t)^\top \quad q_d(t)^\top \quad \dot{q}_d(t)^\top \quad \ddot{q}_d(t)^\top]^\top. \quad (36)$$

Using q_A , we can define a *modified desired velocity trajectory*, \dot{q}_a , and *modified desired acceleration trajectory*, \ddot{q}_a as:

$$\begin{aligned} \dot{q}_a(t) &= \dot{q}_d(t) + K_r e(t), \quad e(t) = q_d(t) - q(t) \\ \ddot{q}_a(t) &= \ddot{q}_d(t) + K_r \dot{e}(t), \quad \dot{e}(t) = \dot{q}_d(t) - \dot{q}(t) \end{aligned} \quad (37)$$

where the gain matrix K_r is a diagonal positive definite matrix. These trajectories do depend on the trajectory parameter $k \in K$; however, we have dropped this dependence for ease of reading in the remainder of the discussion.

The robust passivity-based control input at time $t \in T$ is $u(q_A(t), \Delta_0, [\Delta]) \in \mathbb{R}^{n_q}$, which is composed of a *passivity-based nominal input* $\tau(q_A(t), \Delta_0) \in \mathbb{R}^{n_q}$, as well as a *robust input* $v(q_A(t), \Delta_0, [\Delta]) \in \mathbb{R}^{n_q}$:

$$u(q_A(t), \Delta_0, [\Delta]) = \tau(q_A(t), \Delta_0) - v(q_A(t), \Delta_0, [\Delta]). \quad (38)$$

This decomposition is similar to the one proposed in [35], [51]. The justification for this decomposition is that the nominal control input is unable to perfectly execute the desired trajectory because of a possible mismatch between the nominal inertial parameters Δ_0 and the true parameters Δ . Thus, v is introduced as an additional term to guarantee robustness by compensating for the worst possible disturbances stemming from this mismatch in inertial parameters. Despite the similarities to the decomposition proposed in [35], [51], our formulation of v is distinct and significantly improves upon prior approaches by providing the same tracking error bound while requiring a smaller bound on the robust input v , as is illustrated in [online App. F](#) Next, we define τ and v , and conclude this section by describing how to compute τ and v .

A. Nominal and Robust Controllers

Per Ass. 2, there exists a nominal model of the robot's dynamics given by inertial parameters Δ_0 . Similar to [51], (4)], our nominal input stems from passivity-based control:

$$\begin{aligned} \tau(q_A(t), \Delta_0) &= M(q(t), \Delta_0) \ddot{q}_a(t) + \\ &+ C(q(t), \dot{q}(t), \Delta_0) \dot{q}_a(t) + G(q(t), \Delta_0). \end{aligned} \quad (39)$$

We treat the torques that arise from the possible mismatch between the nominal parameters Δ_0 and the true parameters Δ as a disturbance w , where

$$\begin{aligned} w(q_A(t), \Delta_0, \Delta) &= (M(q(t), \Delta) - M(q(t), \Delta_0)) \ddot{q}_a(t) + \\ &+ (C(q(t), \dot{q}(t), \Delta) - C(q(t), \dot{q}(t), \Delta_0)) \dot{q}_a + \\ &+ G(q(t), \Delta) - G(q(t), \Delta_0). \end{aligned} \quad (40)$$

In practice, w is unknown, but can be bounded by

$$w(q_A(t), \Delta_0, \Delta) \in [w(q_A(t), \Delta_0, [\Delta])], \quad (41)$$

where the right hand side of the previous equation is computed by plugging $[\Delta]$ into (40) in place of Δ and using interval arithmetic. We describe how to compute $[w(q_A(t), \Delta_0, [\Delta])]$ using Alg. 1 in the next subsection.

To create our controller, we next define a function that measures the worst case disturbance:

Definition 7 (Worst Case Disturbance). *Suppose that we have $\inf([w(q_A(t), \Delta_0, [\Delta])]) = \underline{w}$ and $\sup([w(q_A(t), \Delta_0, [\Delta])]) = \bar{w}$. Then the measure of worst case disturbance is the function $\rho: \mathbb{R}^{n_q} \rightarrow \mathbb{R}^{n_q}$ defined as*

$$\rho([w(q_A(t), \Delta_0, [\Delta])]) = \max(|\underline{w}|, |\bar{w}|), \quad (42)$$

where the max operator is applied element-wise.

The absolute value of the disturbance $|w(q_A(t), \Delta_0, \Delta)|$ is always bounded by the worst-case disturbance (42):

Lemma 8 (Disturbance Bound). *For all $q_A(t) \in \mathbb{R}^{6n_q}$ and $\Delta \in [\Delta]$*

$$\rho([w(q_A(t), \Delta_0, [\Delta])]) \geq |w(q_A(t), \Delta_0, \Delta)|, \quad (43)$$

where the inequality is applied element-wise.

Proof. Throughout the proof, we suppress the dependence on $q_A(t)$, Δ , and Δ_0 for convenience. The true disturbance w is contained in the interval $[w]$ as in (41). Therefore, $|w| \in [0, \max(|\underline{w}|, |\bar{w}|)]$. From Def. 7, $\rho([w]) = \max(|\underline{w}|, |\bar{w}|)$, so $\rho([w]) \geq |w|, \forall w \in [w]$. \square

Plugging (38), (39), and (40) into (29) one obtains

$$\begin{aligned} v(q_A(t), \Delta_0, [\Delta]) + w(q_A(t), \Delta_0, \Delta) &= M(q(t), \Delta) \dot{r}(t) + \\ &+ C(q(t), \dot{q}(t), \Delta) r(t) \end{aligned} \quad (44)$$

where $r(t)$ is the *modified tracking error*

$$\begin{aligned} r(t) &= \dot{e}(t) + K_r e(t) \\ \dot{r}(t) &= \ddot{e}(t) + K_r \dot{e}(t). \end{aligned} \quad (45)$$

Our goal is to obtain a uniform bound on the modified tracking error, $r: T \rightarrow \mathbb{R}^{n_q}$. To do this, we make the following assumption about the mass matrix $M(q(t), \Delta)$:

Assumption 9 (Mass Matrix Eigenvalue Bound). *Let $\lambda_m(M(q(t), \Delta))$ and $\lambda_M(M(q(t), \Delta))$ be the minimum and maximum eigenvalues of $M(q(t), \Delta)$. There exist finite uniform bounds $\sigma_m > 0$ and $\sigma_M > 0$ on these eigenvalue so that*

$$0 < \sigma_m \leq \lambda_m(M(q(t), \Delta)) \quad (46)$$

$$0 < \lambda_M(M(q(t), \Delta)) \leq \sigma_M \quad (47)$$

holds for all $q(t) \in Q$ and $\Delta \in [\Delta]$.

Using analysis, one can prove that if $M(q(t), \Delta)$ is positive definite for all $q(t)$ and Δ , then σ_m is at least equal to zero. However proving that this lower bound is greater than zero requires more explicit structure on $[\Delta]$. Because this is not the emphasis of this paper, we make this assumption and verify that it is satisfied numerically during experiments.

We next state a theorem whose proof can be found in App. A that describes how to define the robust input v in (38) by making use of (42) and the previous assumption while ensuring a uniformly bounded tracking error for r .

Theorem 10 (Uniform Tracking Error Bound). *Suppose Ass. 9 is satisfied. Let $V_M > 0$ be a user-specified constant. Consider the following candidate Lyapunov Function*

$$V(q_A(t), \Delta) = \frac{1}{2} r(t)^\top M(q(t), \Delta) r(t). \quad (48)$$

Let \underline{h} be a function that is continuous in its first argument such that

$$\underline{h}(q_A(t), [\Delta]) \leq - \sup_{\Delta^* \in [\Delta]} (V(q_A(t), \Delta^*)) + V_M, \quad (49)$$

for all $q_A(t)$. Let $\alpha : \mathbb{R} \rightarrow \mathbb{R}$ be some extended class \mathcal{K}_∞ function (i.e., $\alpha : \mathbb{R} \rightarrow \mathbb{R}$ is strictly increasing with $\alpha(0) = 0$). Let w_M be any continuous function in its first argument such that

$$w_M(q_A(t), \Delta_0, [\Delta]) \geq \rho([w(q_A(t), \Delta_0, [\Delta])]), \quad (50)$$

for all $q_A(t)$, Δ_0 , and $[\Delta]$, where the inequality is applied element-wise. Suppose that $e(0) = \dot{e}(0) = 0$ and let

$$\varepsilon := \sqrt{\frac{2V_M}{\sigma_m}}. \quad (51)$$

If the robust input is set equal to

$$v(q_A(t), \Delta_0, [\Delta]) = \begin{cases} -\gamma(q_A(t), \Delta_0, [\Delta]) \frac{r(t)}{\|r(t)\|} & \|r(t)\| \neq 0 \\ 0 & \|r(t)\| = 0 \end{cases} \quad (52)$$

with

$$\gamma(q_A(t), \Delta_0, [\Delta]) = \max \left(0, \frac{-\alpha(\underline{h}(q_A(t), [\Delta]))}{\|r(t)\|} + \frac{|r(t)|^\top w_M(q_A(t), \Delta_0, [\Delta])}{\|r(t)\|} \right), \quad (53)$$

then the modified tracking error trajectories $r : T \rightarrow \mathbb{R}^{n_q}$ are uniformly bounded by

$$\|r(t)\| \leq \varepsilon, \quad \forall t \in T \quad (54)$$

when tracking desired trajectories that satisfy Def. 6.

Theorem 10 provides a uniform bound on the tracking error trajectories $r : T \rightarrow \mathbb{R}^{n_q}$. This result can be used to bound the position and velocity tracking errors. The following claim, whose proof can be found in App. B, is inspired by [51, Cor. 6] and [52, Proof of Theorem 2.3], but is distinct because it considers a uniform bound on $r : T \rightarrow \mathbb{R}^{n_q}$ (54) that applies for all T , rather than an ultimate bound that is only valid after some finite time:

Corollary 11 (Tracking Performance). *Suppose Ass. 9 is satisfied and $e(0) = \dot{e}(0) = 0$. If $r : T \rightarrow \mathbb{R}^{n_q}$ is uniformly*

bounded as in (54), then the controller (38) with robust input (52) reaches any desired tracking performance provided a large enough gain matrix K_r . In particular, letting

$$\varepsilon_{p,j} := \frac{\varepsilon}{K_{r,j}} \quad \text{and} \quad (55)$$

$$\varepsilon_v := 2\varepsilon, \quad (56)$$

where ε as in (51) and $K_{r,j}$ is the j^{th} element of the diagonal gain matrix K_r , then $|e_j(t)| \leq \varepsilon_{p,j}$ and $|\dot{e}_j(t)| \leq \varepsilon_v$ for all $t \in T$ and $j \in N_q$.

Though these bounds can be made arbitrarily small by either increasing K_r or decreasing V_m , satisfying these bounds may require large torques, causing input saturation. In Sec. VIII, we explain how to overapproximate the torques required to track a given desired trajectory including all possible tracking error.

Before proceeding further, we make one final remark about the validity of these bounds for all time.

Remark 12 (Error Bound for All Time). *By Def. 4, the robot starts from configuration q_{start} with zero initial velocity and acceleration. Suppose that the initial condition of the desired trajectory in the first planning iteration matches this (i.e., $q_{d_0} = q_{\text{start}}$, $\dot{q}_{d_0} = 0$, $\ddot{q}_{d_0} = 0$), and that the initial condition of all subsequent desired trajectories match the state of the previous desired trajectory at $t = t_p$. Then, one can satisfy the bounds described in Thm. 10 and Cor. 11 for all time.*

This remark follows directly from the proofs of Thm. 10 and Cor. 11 by noticing that the arguments in their proofs hold for desired trajectories that are defined for all time rather than just for $t \in T$. One can create a valid desired trajectory defined for all time by applying the strategy described in Rem. 12. This is the approach we adopt while performing receding horizon planning as described in Sec. VIII. To apply Rem. 12, one only needs to know the final state of the previous *desired trajectory* rather than the final state of the robot's *actual trajectory*.

B. Controller Implementation

The Interval Recursive Newton Euler Algorithm (IRNEA), introduced in [35], can be applied to compute the the nominal and robust inputs. IRNEA is described in Alg. 1, where we have suppressed the dependence on $q_j(t)$ in R_j^{i-1} and p_j^{i-1} for convenience. The primary distinction between the classical Recursive Newton Euler Algorithm (RNEA) and IRNEA is that the latter takes in an interval set of inertial parameters and performs interval arithmetic in place of standard arithmetic. One can apply IRNEA to compute τ :

$$\tau(q_A(t), \Delta_0) = \text{IRNEA}(q_A(t), \Delta_0, a_0^0) \quad (57)$$

where $a_0^0 = (0, 0, 9.81)^\top$ accounts for the effect of gravity. By passing the nominal parameters Δ_0 (i.e., a degenerate interval) to IRNEA, the interval arithmetic in Alg. 1 become standard arithmetic and IRNEA is identical to RNEA. Computing v requires computing bounds on the worst-case disturbance $w_M(q_A(t), \Delta_0, [\Delta])$ and on the function $\underline{h}(q_A(t), [\Delta])$. The following lemma, whose proof can be found in App. C, describes how to use Alg. 1 to compute w_M and a \underline{h} to satisfy the

Algorithm 1:

```

{[uj(t, [Δ])]: j ∈ Nq} = IRNEA(qA(t), [Δ], a00)
1: Compute  $\dot{q}_a(t)$  and  $\ddot{q}_a(t)$  using (37).
2: Initialize base linear acceleration  $a_0^0$ .
3: for j = 1 : nq // for each joint
4:    $R_j^{j-1}, p_j^{j-1} \leftarrow H_j^{j-1}(q_j(t))$  as in (22)
5:    $R_{j-1}^j \leftarrow \text{transpose}(R_j^{j-1})$ 
6: end for
7: for j = 1 : nq // for each joint (forward recursion)
8:    $\omega_j^j \leftarrow R_{j-1}^j \omega_{j-1}^{j-1} + \dot{q}_j(t) \hat{z}_j$ 
9:    $\omega_{a,j}^j \leftarrow R_{j-1}^j \omega_{a,j-1}^{j-1} + \dot{q}_{a,j}(t) \hat{z}_j$ 
10:   $\dot{\omega}_j^j \leftarrow R_{j-1}^j \dot{\omega}_{j-1}^{j-1} + ((R_{j-1}^j \omega_{a,j-1}^{j-1}) \times (\dot{q}_j(t) \hat{z}_j)) + \ddot{q}_{a,j}(t) \hat{z}_j$ 
11:   $a_j^j \leftarrow (R_{j-1}^j a_{j-1}^{j-1}) + (\dot{\omega}_j^j \times p_j^{j-1}) + (\omega_j^j \times (\omega_{a,j}^j \times p_j^{j-1}))$ 
12:   $[a_{c,j}^j] \leftarrow a_j^j + (\dot{\omega}_j^j \otimes [c_j^j]) + (\omega_j^j \otimes (\omega_{a,j}^j \otimes [c_j^j]))$ 
13:   $[F_j^j] \leftarrow [m_i][a_{c,j}^j]$ 
14:   $[N_j^j] \leftarrow [I_j^j] \dot{\omega}_j^j \oplus (\omega_{a,j}^j \otimes ([I_j^j] \omega_j^j))$ 
15: end for
16:  $R_{n_q+1}^{n_q} \leftarrow I_{3 \times 3}$ 
17:  $[J_{n_q+1}^{n_q+1}] \leftarrow 0$ 
18:  $[n_{n_q+1}^{n_q+1}] \leftarrow 0$ 
19: for j = nq : -1 : 1 // for each joint (backward recursion)
20:   $[f_j^j] \leftarrow (R_{j+1}^j [f_{j+1}^{j+1}]) \oplus [F_j^j]$ 
21:   $[n_j^j] \leftarrow (R_{j+1}^j [n_{j+1}^{j+1}]) \oplus ([c_j^j] \otimes [F_j^j]) \oplus$ 
     $\oplus (p_{j-1}^j \otimes (R_{j+1}^j [f_{j+1}^{j+1}])) \oplus [N_j^j]$ 
22:   $[u_j(t, [\Delta])] \leftarrow \hat{z}_j^\top [n_j^j]$ 
23: end for

```

requirements of Thm. 10 and thereby compute the robust passivity-based controller.

Lemma 13 (Computing the Robust Input). *If the interval disturbance in (40) is computed as:*

$$[w(q_A(t), \Delta_0, [\Delta])] = \text{IRNEA}(q_A(t), [\Delta], a_0^0) - \tau(q_A(t), \Delta_0), \quad (58)$$

and we define w_M using the previous equation as:

$$w_M(q_A(t), \Delta_0, [\Delta]) := \rho([w(q_A(t), \Delta_0, [\Delta])]), \quad (59)$$

where ρ is as in Def. 7, then w_M satisfies (50) and is continuous in its first argument. Similarly, let

$$[V(q_A(t), [\Delta])] = \frac{1}{2} r(t)^\top [M(q(t), [\Delta]) r(t)]. \quad (60)$$

The term $[M(q(t), [\Delta]) r(t)]$ can be computed as

$$[M(q(t), [\Delta]) r(t)] = \text{IRNEA}(q_R(t), [\Delta], 0) \quad (61)$$

where $q_R(t)$ is defined as

$$q_R(t) = [q(t)^\top \quad 0^\top \quad q(t)^\top \quad 0^\top \quad r(t)^\top]^\top \quad (62)$$

and the base acceleration is set to 0. If \underline{h} is defined as:

$$\underline{h}(q_A(t), [\Delta]) = -(\text{sup}([V(q_A(t), [\Delta])])) + V_M, \quad (63)$$

then it satisfies (49) and is continuous in its first argument.

VIII. PLANNING ALGORITHM FORMULATION

One of the key ideas of this work is to generate polynomial zonotope overapproximations of the trajectory and all constraints in the optimization problem (31)-(35) at the start of the planning iteration, then use these constraint overapproximations to perform optimization within t_p . Our approach guarantees safety while also ensuring:

- I. **Speed:** the size of all polynomial zonotope constraints can be fixed *a priori*, ensuring fast constraint evaluation, and analytical gradients are generated via polynomial differentiation for use in optimization.
- II. **Continuous time and tracking error intervals:** each constraint is satisfied over the entire trajectory (including tracking error) for all time $t \in T$ rather than just at discretized time instances.
- III. **Physical consistency:** dependencies between uncertain inertial parameters can be modeled explicitly using polynomial zonotopes.

This section presents the theory to transform the optimization problem (31)-(35) into an implementable version whose solutions can be followed by the robot in a dynamically feasible and collision free fashion.

A. Polynomial Zonotope Trajectory Representation

As illustrated in Fig. 4, this subsection describes how AR-MOUR overapproximates parameterized desired trajectories, as in Def. 6, to conservatively account for continuous time and tracking error. Because of Rem. 12, the initial condition of the desired trajectories at each planning iteration is known, so the desired trajectories are functions of time and the trajectory parameter. We create polynomial zonotope versions of T and K that are then plugged into the desired trajectory to create polynomial zonotopes representing the desired trajectories.

1) *Time Horizon PZs:* We first create polynomial zonotopes representing the time horizon T . Choose a timestep Δt so that $n_t := \frac{T}{\Delta t} \in \mathbb{N}$. Let $N_t := \{1, \dots, n_t\}$. Divide the compact time horizon $T \subset \mathbb{R}$ into n_t time subintervals. Consider the i^{th} time subinterval corresponding to $t \in [(i-1)\Delta t, i\Delta t]$. We represent this subinterval as a polynomial zonotope \mathbf{T}_i , where

$$\mathbf{T}_i = \left\{ t \in T \mid t = \frac{(i-1)+i}{2} \Delta t + \frac{1}{2} \Delta t x_i, x_i \in [-1, 1] \right\} \quad (64)$$

with indeterminate $x_i \in [-1, 1]$.

2) *Trajectory Parameter PZs:* Next, we describe how to create polynomial zonotopes representing the set of trajectory parameters K . This work chooses $K = \times_{i=1}^{n_q} K_i$, where each K_j is a compact one-dimensional interval. For simplicity, we let each $K_j = [-1, 1]$. We represent the interval K_j as a polynomial zonotope $\mathbf{K}_j = x_{k_j}$ where $x_{k_j} \in [-1, 1]$ is an indeterminate. We let $x_k \in [-1, 1]^{n_q}$ denote the vector of indeterminates where the j^{th} component of x_k is x_{k_j} . With this choice of K_j , any particular k_j yields $k_j = \text{slice}(\mathbf{K}_j, x_{k_j}, k_j)$ (see (13)).

3) *Desired Trajectory PZs:* Next, we create polynomial zonotopes $\mathbf{q}_{d,j}(\mathbf{T}_i; \mathbf{K})$ that overapproximate $q_{d,j}(t; k)$ for all t in the i^{th} time subinterval and $k \in K$ by plugging the polynomial zonotopes \mathbf{T}_i and \mathbf{K} into $q_{d,j}(t; k)$ (see second column of Fig. 4).

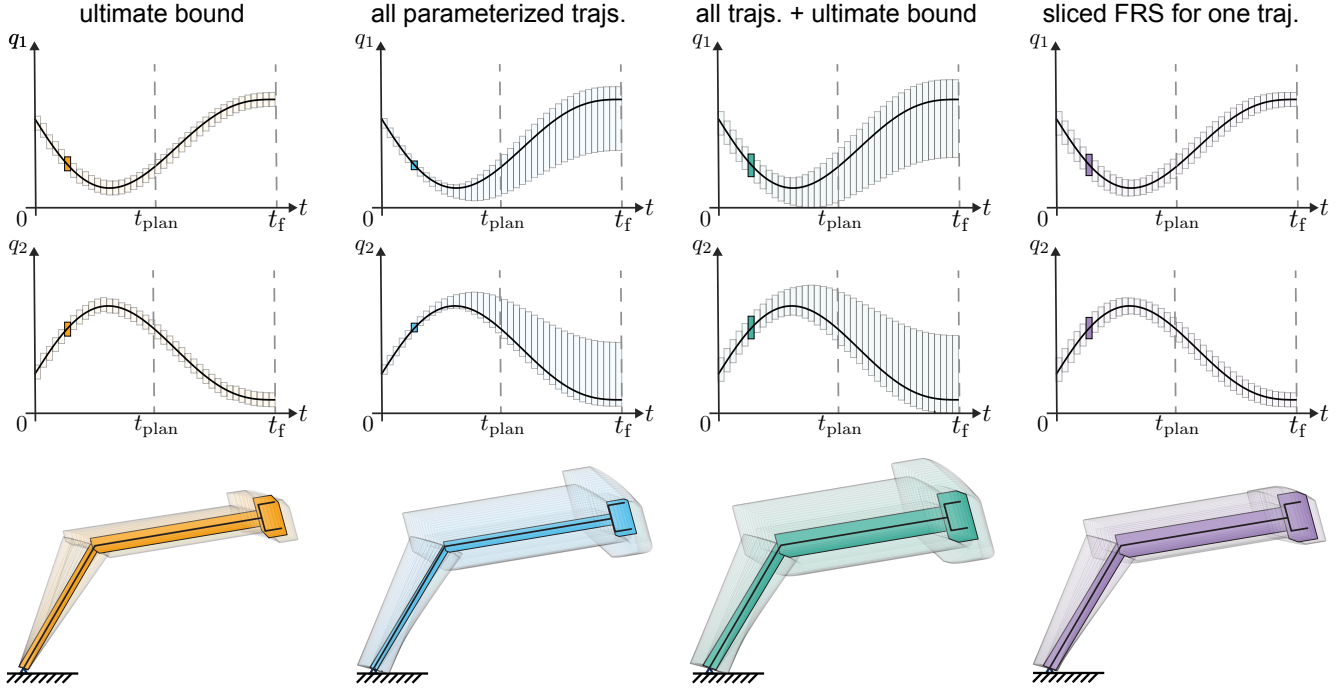


Fig. 4. A visualization of how the polynomial zonotope trajectory representation is used to construct the polynomial zonotope forward occupancy for a two link arm in 2D. A desired trajectory for each joint is shown in black in the top two rows. The same desired trajectory is depicted in each column. The planning time horizon is partitioned into a finite set of polynomial zonotopes (Sec. VIII-A1). In each column, a single time interval is highlighted in the top two rows and the corresponding time instance is highlighted in the visualization in the bottom row. The top two rows of the first column depicts a finite set of polynomial zonotopes generated by uniformly buffering a desired trajectory by the ultimate bound (Lem. 16). The bottom row of the first column depicts the forward occupancy of the robot over this entire set (Lem. 18). The second column depicts a family of desired trajectories that are overapproximated by a finite set of polynomial zonotopes and the corresponding forward occupancy of the robot over this entire set. The third column depicts a family of desired trajectories buffered by the ultimate bound that are overapproximated by a finite set of polynomial zonotopes and the corresponding forward occupancy of the robot over this entire set. The fourth column depicts a subset of the sets illustrated in the third column generated by slicing in a specific trajectory parameter (Sec. VIII-A4). Note that the desired trajectory always remains within the polynomial zonotope overapproximations.

Lemma 14 (Desired Trajectory PZs). *The desired trajectory polynomial zonotopes $\mathbf{q}_{d,j}(\mathbf{T}_i; \mathbf{K})$ are overapproximative, i.e., for each $j \in N_q$,*

$$q_{d,j}(t;k) \in \mathbf{q}_{d,j}(\mathbf{T}_i; \mathbf{K}), \quad \forall t \in \mathbf{T}_i, k \in \mathbf{K}. \quad (65)$$

One can similarly define $\dot{\mathbf{q}}_{d,j}(\mathbf{T}_i; \mathbf{K})$, and $\ddot{\mathbf{q}}_{d,j}(\mathbf{T}_i; \mathbf{K})$ that are overapproximative.

Proof. $q_{d,j}$ is an analytic function that depends only on t and k , which are included in \mathbf{T}_i and \mathbf{K} . All operations involving polynomial zonotopes are either exact or overapproximative for analytic functions [2, Sec. 2.D], so \mathbf{T}_i and \mathbf{K} in place of t and k yields an overapproximative polynomial zonotope. \square

To illustrate how the polynomial zonotope representation works, consider the following example:

Example 15. *Suppose we parameterize the desired trajectories using degree 5 Bernstein polynomials. Letting $T = [0, 1]$, the Bernstein polynomials take the form*

$$q_{d,j}(t;k) = \sum_{l=0}^5 \beta_{j,l}(k) b_{j,l}(t), \quad (66)$$

where $\beta_{j,l}(k) \in \mathbb{R}$ are the Bernstein Coefficients and $b_{j,l}: T \rightarrow \mathbb{R}$ are the Bernstein Basis Polynomials of degree 5 given by

$$b_{j,l}(t) = \binom{5}{l} t^l (1-t)^{5-l}, \quad (67)$$

for each $l \in \{0, \dots, 5\}$. From Def. 6 the first and second properties of trajectory parameters constrain the initial position, velocity, and acceleration of the trajectory to match the initial condition, and require the final velocity and acceleration to be 0. These properties fix five of the six Bernstein coefficients $\beta_{j,v}$ as $\beta_{j,0}(k) = q_{d,j,0}$, $\beta_{j,1}(k) = \frac{1}{5}(\dot{q}_{d,j,0} + 5\beta_{j,0})$, $\beta_{j,2}(k) = \frac{1}{20}(\ddot{q}_{d,j,0} + 40\beta_{j,1} - 20\beta_{j,0})$, $\beta_{j,3}(k) = \frac{1}{20}(0 + 40\beta_{j,4} - 20\beta_{j,5})$, and $\beta_{j,4}(k) = \frac{1}{5}(0 + 5\beta_{j,5})$. Because the first five Bernstein coefficients are fixed, we drop the dependence on k for these coefficients. We choose the last coefficient as

$$\beta_{j,5}(k) = \eta_{j,1}k_j + \eta_{j,2} \quad (68)$$

where $\eta_{j,1}$ and $\eta_{j,2} \in \mathbb{R}$ are user-specified constants. The coefficient $\beta_{j,5}$ equals the final position $q_{d,j}(1;k)$ at time $t = 1$, so the choice of trajectory parameter k_j determines this value.

Construct the polynomial zonotope representation $\mathbf{q}_{d,j}(\mathbf{T}_i; \mathbf{K})$ by plugging in \mathbf{T}_i from (64) and \mathbf{K}_j . Letting $\beta_{j,5}(\mathbf{K}) = \eta_{j,1}\mathbf{K}_j + \eta_{j,2}$, and plugging \mathbf{T}_i into the basis polynomials (67), we obtain

$$\mathbf{q}_{d,j}(\mathbf{T}_i; \mathbf{K}) = \left(\sum_{l=0}^4 \beta_{j,l} \mathbf{b}_{j,l}(\mathbf{T}_i) \right) \oplus \beta_{j,5}(\mathbf{K}) \mathbf{b}_{j,5}(\mathbf{T}_i), \quad (69)$$

The desired velocity and acceleration polynomial zonotopes $\dot{\mathbf{q}}_{d,j}(\mathbf{T}_i; \mathbf{K})$ and $\ddot{\mathbf{q}}_{d,j}(\mathbf{T}_i; \mathbf{K})$ can be similarly computed.

4) *Slicing Yields Desired Trajectories*: \mathbf{T}_i and \mathbf{K}_j have indeterminates x_{t_i} and x_{k_j} respectively. Because the desired trajectories only depend on t and k , the polynomial zonotopes $\mathbf{q}_{d,j}(\mathbf{T}_i; \mathbf{K})$, $\dot{\mathbf{q}}_{d,j}(\mathbf{T}_i; \mathbf{K})$ and $\ddot{\mathbf{q}}_{d,j}(\mathbf{T}_i; \mathbf{K})$ depend only on the indeterminates x_{t_i} and x_{k_j} . By plugging in a given k for x_{k_j} via the `slice` operation, we obtain a polynomial zonotope where x_{t_i} is the only remaining indeterminate. Because we perform this slicing operation throughout this document, we use the shorthand $\mathbf{q}_{d,j}(\mathbf{T}_i; k) = \text{slice}(\mathbf{q}_{d,j}(\mathbf{T}_i; \mathbf{K}), x_{k_j}, k)$ for a given polynomial zonotope, $\mathbf{q}_{d,j}(\mathbf{T}_i; \mathbf{K})$. Because of our previous observation, $q_{d,j}(t; k) \in \mathbf{q}_{d,j}(\mathbf{T}_i; k)$ for all $t \in \mathbf{T}_i$ (and similarly for $\dot{\mathbf{q}}_{d,j}(\mathbf{T}_i; k)$ and $\ddot{\mathbf{q}}_{d,j}(\mathbf{T}_i; k)$).

5) *Incorporating Tracking Error*: Recall from Sec. VII that desired trajectories may not be tracked perfectly. As depicted in the first and third column of Fig. 4, by applying Cor. 11 and Lem. 14, we can overapproximate any trajectory followed by the robot:

Lemma 16 (Error in Config. Space). *Let $\boldsymbol{\varepsilon}_{p,j} = \varepsilon_{p,j} x_{e_{p,j}}$ and $\boldsymbol{\varepsilon}_{v,j} = \varepsilon_{v,j} x_{e_{v,j}}$, with indeterminates $x_{e_{p,j}} \in [-1, 1]$ and $x_{e_{v,j}} \in [-1, 1]$. Then, for each $i \in N_t$ let*

$$\mathbf{q}_j(\mathbf{T}_i; \mathbf{K}) = \mathbf{q}_{d,j}(\mathbf{T}_i; \mathbf{K}) \oplus \boldsymbol{\varepsilon}_{p,j} \quad (70)$$

$$\dot{\mathbf{q}}_j(\mathbf{T}_i; \mathbf{K}) = \dot{\mathbf{q}}_{d,j}(\mathbf{T}_i; \mathbf{K}) \oplus \boldsymbol{\varepsilon}_{v,j}. \quad (71)$$

Given the set of trajectory parameters \mathbf{K} , the polynomial zonotopes $\mathbf{q}_j(\mathbf{T}_i; \mathbf{K})$ and $\dot{\mathbf{q}}_j(\mathbf{T}_i; \mathbf{K})$ overapproximate the set of all joint trajectories that can possibly be executed by the robot, i.e., for each $j \in N_q$, $k \in \mathbf{K}$ we have

$$q_j(t; k) \in \mathbf{q}_j(\mathbf{T}_i; k), \quad \forall t \in \mathbf{T}_i \quad (72)$$

$$\dot{q}_j(t; k) \in \dot{\mathbf{q}}_j(\mathbf{T}_i; k), \quad \forall t \in \mathbf{T}_i. \quad (73)$$

Moving forward, let $\mathbf{q}_d(\mathbf{T}_i; \mathbf{K}) = \times_{j=1}^{n_q} \mathbf{q}_{d,j}(\mathbf{T}_i; \mathbf{K})$, and similarly define $\mathbf{q}(\mathbf{T}_i; \mathbf{K})$, $\dot{\mathbf{q}}_d(\mathbf{T}_i; \mathbf{K})$, $\dot{\mathbf{q}}(\mathbf{T}_i; \mathbf{K})$, $\ddot{\mathbf{q}}_d(\mathbf{T}_i; \mathbf{K})$, and $\ddot{\mathbf{q}}(\mathbf{T}_i; \mathbf{K})$. Furthermore, let $\boldsymbol{\varepsilon}_p = \times_{j=1}^{n_q} \boldsymbol{\varepsilon}_{p,j}$, and similarly define $\boldsymbol{\varepsilon}_v$ using $\boldsymbol{\varepsilon}_{v,j}$.

B. Reachable Set Construction

Next, ARMOUR bounds the kinematic behavior of the arm and the possible torques required to track a trajectory. These bounds are then used to formulate constraints on k that overapproximate those in (32) - (35).

1) *Forward Kinematics Reachable Set*: We represent the robot's forward kinematics (23) using polynomial zonotope overapproximations of the joint position trajectories. Using $\mathbf{q}_j(\mathbf{T}_i; \mathbf{K})$, we compute $\mathbf{p}_j^{j-1}(\mathbf{q}_j(\mathbf{T}_i; \mathbf{K}))$ and $\mathbf{R}_j^{j-1}(\mathbf{q}_j(\mathbf{T}_i; \mathbf{K}))$, which represent overapproximations of the position and orientation of the j^{th} frame with respect to frame $(j-1)$ at the i^{th} time step. The rotation matrix $R_j^{j-1}(q_j(t; k))$ depends on $\cos(q_j(t; k))$ and $\sin(q_j(t; k))$. As a result, we must compute $\cos(\mathbf{q}_j(\mathbf{T}_i; \mathbf{K}))$ and $\sin(\mathbf{q}_j(\mathbf{T}_i; \mathbf{K}))$ to compute $\mathbf{R}_j^{j-1}(\mathbf{q}_j(\mathbf{T}_i; \mathbf{K}))$. Cosine and sine are analytic functions, so we compute $\cos(\mathbf{q}_j(\mathbf{T}_i; \mathbf{K}))$ and $\sin(\mathbf{q}_j(\mathbf{T}_i; \mathbf{K}))$ using Taylor expansions as in Sec. III-C. Because all operations involving polynomial zonotopes are either exact or overapproximative, the polynomial zonotope forward kinematics can be computed similarly to the classical formulation (23) and proven to be overapproximative:

Algorithm 2: $\{\text{FK}_j(\mathbf{q}(\mathbf{T}_i; \mathbf{K})) : j \in N_q\} = \text{PZFK}(\mathbf{q}(\mathbf{T}_i; \mathbf{K}))$

```

1:  $\mathbf{p}_0(\mathbf{q}(\mathbf{T}_i; \mathbf{K})) \leftarrow 0$ 
2:  $\mathbf{R}_0(\mathbf{q}(\mathbf{T}_i; \mathbf{K})) \leftarrow I_{3 \times 3}$ 
3: for  $j = 1 : n_q$ 
4:    $\mathbf{R}_j^{j-1}(\mathbf{q}_j(\mathbf{T}_i; \mathbf{K})), \mathbf{p}_j^{j-1} \leftarrow \mathbf{H}_j^{j-1}(\mathbf{q}_j(\mathbf{T}_i; \mathbf{K}))$  as in (22)
5:    $\mathbf{p}_j(\mathbf{q}(\mathbf{T}_i; \mathbf{K})) \leftarrow \mathbf{p}_{j-1}(\mathbf{q}(\mathbf{T}_i; \mathbf{K})) \oplus \mathbf{R}_{j-1}(\mathbf{q}(\mathbf{T}_i; \mathbf{K})) \mathbf{p}_j^{j-1}$ 
6:    $\mathbf{R}_j(\mathbf{q}(\mathbf{T}_i; \mathbf{K})) \leftarrow \mathbf{R}_{j-1}(\mathbf{q}(\mathbf{T}_i; \mathbf{K})) \mathbf{R}_j^{j-1}(\mathbf{q}_j(\mathbf{T}_i; \mathbf{K}))$ 
7:    $\text{FK}_j(\mathbf{q}(\mathbf{T}_i; \mathbf{K})) \leftarrow \{\mathbf{R}_j(\mathbf{q}(\mathbf{T}_i; \mathbf{K})), \mathbf{p}_j(\mathbf{q}(\mathbf{T}_i; \mathbf{K}))\}$ 
8: end for

```

Lemma 17 (PZ Forward Kinematics). *Let the polynomial zonotope forward kinematics for the j^{th} frame at the i^{th} time step be defined as*

$$\text{FK}_j(\mathbf{q}(\mathbf{T}_i; \mathbf{K})) = \begin{bmatrix} \mathbf{R}_j(\mathbf{q}(\mathbf{T}_i; \mathbf{K})) & \mathbf{p}_j(\mathbf{q}(\mathbf{T}_i; \mathbf{K})) \\ \mathbf{0} & \mathbf{1} \end{bmatrix}, \quad (74)$$

where

$$\mathbf{R}_j(\mathbf{q}(\mathbf{T}_i; \mathbf{K})) = \prod_{l=1}^j \mathbf{R}_l^{l-1}(\mathbf{q}_l(\mathbf{T}_i; \mathbf{K})), \quad (75)$$

$$\mathbf{p}_j(\mathbf{q}(\mathbf{T}_i; \mathbf{K})) = \sum_{l=1}^j \mathbf{R}_l(\mathbf{q}(\mathbf{T}_i; \mathbf{K})) \mathbf{p}_l^{l-1}, \quad (76)$$

then for each $j \in N_q$, $k \in \mathbf{K}$, $\text{FK}_j(q(t; k)) \in \text{FK}_j(\mathbf{q}(\mathbf{T}_i; k))$ for all $t \in \mathbf{T}_i$.

The Polynomial Zonotope Forward Kinematics Algorithm (PZFK), detailed in Alg. 2, is used to compute the objects in Lem. 17 from the set of possible configurations $\mathbf{q}(\mathbf{T}_i; \mathbf{K})$.

2) *Forward Occupancy Reachable Set*: To ensure that the robot never collides with any obstacles, we overapproximate the forward occupancy (26) of each link over every time interval. By applying the polynomial zonotope forward kinematics set and the fact that all operations involving polynomial zonotopes are either exact or overapproximative, the polynomial zonotope forward occupancy reachable set can be computed and proven to be overapproximative:

Lemma 18 (PZ Forward Occupancy). *Let the j^{th} link of the robot be overapproximated by a polynomial zonotope denoted by \mathbf{L}_j and the polynomial zonotope forward occupancy reachable set for the j^{th} link at the i^{th} time step be defined as:*

$$\text{FO}_j(\mathbf{q}(\mathbf{T}_i; \mathbf{K})) = \mathbf{p}_j(\mathbf{q}(\mathbf{T}_i; \mathbf{K})) \oplus \mathbf{R}_j(\mathbf{q}(\mathbf{T}_i; \mathbf{K})) \mathbf{L}_j, \quad (77)$$

then for each $j \in N_q$, $k \in \mathbf{K}$, $\text{FO}_j(q(t; k)) \in \text{FO}_j(\mathbf{q}(\mathbf{T}_i; k))$ for all $t \in \mathbf{T}_i$.

Sec. VIII-C describes how the forward occupancy reachable set is used to compute collision-avoidance constraints. Let

$$\text{FO}(\mathbf{q}(\mathbf{T}_i; \mathbf{K})) = \bigcup_{j=1}^{n_q} \text{FO}_j(\mathbf{q}(\mathbf{T}_i; \mathbf{K})). \quad (78)$$

3) *Input Reachable Set*: Mobile manipulators must also avoid saturating their available motor torques. We describe how to overapproximate the set of torques that may be required for the robust passivity-based control input (38) to track any parameterized trajectory. Just as we did in Sec. VII, we define a total feedback trajectory polynomial zonotope $\mathbf{q}_A(\mathbf{T}_i; \mathbf{K})$ by

Algorithm 3:

$$\{\mathbf{u}_j(\mathbf{q}_A(\mathbf{T}_i; \mathbf{K}), [\Delta]) : j \in N_q\} = \text{PZRNEA}(\mathbf{q}_A(\mathbf{T}_i; \mathbf{K}), [\Delta], a_0^0)$$

```

1: Compute  $\hat{\mathbf{q}}_a(\mathbf{T}_i; \mathbf{K})$  and  $\hat{\mathbf{q}}_a(\mathbf{T}_i; \mathbf{K})$  using (79)
2: Initialize base acceleration  $a_0^0$ .
3: for  $j = 1 : n_q$ 
4:    $\mathbf{R}_j^{j-1}, \mathbf{p}_j^{j-1} \leftarrow \mathbf{H}_j^{j-1}(\mathbf{q}_j(\mathbf{T}_i; \mathbf{K}))$ 
5:    $\mathbf{R}_{j-1}^j \leftarrow \text{pzTranspose}(\mathbf{R}_j^{j-1})$ 
6: end for
7: for  $j = 1 : n_q$ 
8:    $\omega_j^j \leftarrow \mathbf{R}_{j-1}^j \omega_{j-1}^{j-1} \oplus \hat{\mathbf{q}}_j(t) \hat{z}_j$ 
9:    $\omega_{a,j}^j \leftarrow \mathbf{R}_{j-1}^j \omega_{a,j-1}^{j-1} \oplus \hat{\mathbf{q}}_{a,j}(t) \hat{z}_j$ 
10:   $\hat{\omega}_j^j \leftarrow \mathbf{R}_{j-1}^j \hat{\omega}_{j-1}^{j-1} \oplus ((\mathbf{R}_{j-1}^j \omega_{a,j-1}^{j-1}) \otimes (\hat{\mathbf{q}}_j(t) \hat{z}_j)) \oplus \hat{\mathbf{q}}_{a,j} \hat{z}_j$ 
11:   $\mathbf{a}_j^j \leftarrow (\mathbf{R}_{j-1}^j \mathbf{a}_{j-1}^{j-1}) \oplus (\hat{\omega}_j^j \otimes \mathbf{p}_j^{j-1}) \oplus (\omega_j^j \otimes (\omega_{a,j}^j \times \mathbf{p}_j^{j-1}))$ 
12:   $\mathbf{a}_{c,j}^j \leftarrow \mathbf{a}_j^j \oplus (\hat{\omega}_j^j \otimes \mathbf{c}_j^j) \oplus (\omega_j^j \otimes (\omega_{a,j}^j \otimes \mathbf{c}_j^j))$ 
13:   $\mathbf{F}_j^j \leftarrow \mathbf{m}_j \mathbf{a}_{c,j}^j$ 
14:   $\mathbf{N}_j^j \leftarrow \mathbf{I}_j^j \hat{\omega}_j^j \oplus (\omega_{a,j}^j \otimes (\mathbf{I}_j^j \omega_j^j))$ 
15: end for
16:  $\mathbf{R}_{n_q+1}^{n_q} \leftarrow \mathbf{I}_{3 \times 3}$ 
17:  $\mathbf{f}_{n_q+1}^{n_q+1} \leftarrow 0$ 
18:  $\mathbf{n}_{n_q+1}^{n_q+1} \leftarrow 0$ 
19: for  $j = n_q : -1 : 1$ 
20:    $\mathbf{f}_j^j \leftarrow (\mathbf{R}_{j+1}^j \mathbf{f}_{j+1}^{j+1}) \oplus \mathbf{F}_j^j$ 
21:    $\mathbf{n}_j^j \leftarrow (\mathbf{R}_{j+1}^j \mathbf{n}_{j+1}^{j+1}) \oplus (\mathbf{c}_j^j \otimes \mathbf{F}_j^j) \oplus$ 
       $\oplus (\mathbf{p}_{j-1}^j \otimes (\mathbf{R}_{j+1}^j \mathbf{f}_{j+1}^{j+1})) \oplus \mathbf{N}_j^j$ 
22:    $\mathbf{u}_j(\mathbf{q}_A(\mathbf{T}_i; \mathbf{K}), [\Delta]) \leftarrow \hat{z}_j^T \mathbf{n}_j^j$ 
23: end for

```

computing a polynomial zonotope representation of each of the components of q_A . We similarly define modified desired velocity and acceleration trajectory polynomial zonotopes:

$$\begin{aligned} \hat{\mathbf{q}}_a(\mathbf{T}_i; \mathbf{K}) &= \mathbf{q}_d(\mathbf{T}_i; \mathbf{K}) \oplus K_r \mathbf{E}_p, \\ \hat{\mathbf{q}}_a(\mathbf{T}_i; \mathbf{K}) &= \hat{\mathbf{q}}_d(\mathbf{T}_i; \mathbf{K}) \oplus K_r \mathbf{E}_v. \end{aligned} \quad (79)$$

Using these definitions and plugging into (39), we obtain

$$\begin{aligned} \boldsymbol{\tau}(\mathbf{q}_A(\mathbf{T}_i; \mathbf{K}), \Delta_0) &= \mathbf{M}(\mathbf{q}(\mathbf{T}_i; \mathbf{K}), \Delta_0) \hat{\mathbf{q}}_a(\mathbf{T}_i; \mathbf{K}) + \\ &+ \mathbf{C}(\mathbf{q}(\mathbf{T}_i; \mathbf{K}), \hat{\mathbf{q}}(\mathbf{T}_i; \mathbf{K}), \Delta_0) \hat{\mathbf{q}}_a(\mathbf{T}_i; \mathbf{K}) + \\ &+ \mathbf{G}(\mathbf{q}(\mathbf{T}_i; \mathbf{K}), \Delta_0). \end{aligned} \quad (80)$$

To compute $\boldsymbol{\tau}(\mathbf{q}_A(\mathbf{T}_i; \mathbf{K}), \Delta_0)$, we introduce the Polynomial Zonotope RNEA (PZRNEA), detailed in Alg. 3. Note just as in the original RNEA and IRNEA Algorithms, we have suppressed the dependence on $\mathbf{q}_j(\mathbf{T}_i; \mathbf{K})$ in \mathbf{R}_{j-1}^j . PZRNEA takes as inputs $\mathbf{q}_A(\mathbf{T}_i; \mathbf{K})$, and the nominal inertial parameters Δ_0 to find the nominal input:

$$\boldsymbol{\tau}(\mathbf{q}_A(\mathbf{T}_i; \mathbf{K}), \Delta_0) = \text{PZRNEA}(\mathbf{q}_A(\mathbf{T}_i; \mathbf{K}), \Delta_0, a_0^0), \quad (81)$$

where $a_0^0 = [0, 0, 9.81]^\top$.

Next, we describe a bound on the robust control input (52) at each time step whose proof can be found in App. E.

Theorem 19 (Robust Input Bound). *Suppose $\alpha : \mathbb{R} \rightarrow \mathbb{R}$ in (53) is a linear function, i.e., $\alpha(x) = \alpha_c x$, where $\alpha_c > 0$ is a*

user-specified constant. Suppose as in (58), the disturbance (40) is overapproximated using

$$\begin{aligned} \mathbf{w}(\mathbf{q}_A(\mathbf{T}_i; \mathbf{K}), \Delta_0, [\Delta]) &= \text{PZRNEA}(\mathbf{q}_A(\mathbf{T}_i; \mathbf{K}), [\Delta], a_0^0) + \\ &- \boldsymbol{\tau}(\mathbf{q}_A(\mathbf{T}_i; \mathbf{K}), \Delta_0) \end{aligned} \quad (82)$$

with PZRNEA as in Alg. 3 and $a_0^0 = [0, 0, 9.81]^\top$. Using Def. 7, let

$$\begin{aligned} \rho(\mathbf{w}(\mathbf{q}_A(\mathbf{T}_i; \mathbf{K}), \Delta_0, [\Delta])) &= \max \left(\left| \inf(\mathbf{w}(\mathbf{q}_A(\mathbf{T}_i; \mathbf{K}), \Delta_0, [\Delta])) \right|, \right. \\ &\left. \left| \sup(\mathbf{w}(\mathbf{q}_A(\mathbf{T}_i; \mathbf{K}), \Delta_0, [\Delta])) \right| \right), \end{aligned} \quad (83)$$

and as in (59) let

$$w_M(\ast) = \rho(\mathbf{w}(\mathbf{q}_A(\mathbf{T}_i; \mathbf{K}), \Delta_0, [\Delta])) \quad (84)$$

where $w_M(\ast) := w_M(\mathbf{q}_A(\mathbf{T}_i; \mathbf{K}), \Delta_0, [\Delta])$. Then for all $q_A(t; k)$ that satisfies the uniform bound (54), the following bound is satisfied for each $j \in N_q$

$$\begin{aligned} |v(q_A(t; k), \Delta_0, [\Delta])_j| &\leq \frac{\alpha_c \mathcal{E}(\sigma_M - \sigma_m)}{2} + \\ &+ \frac{\|w_M(\ast)\| + w_M(\ast)_j}{2}, \end{aligned} \quad (85)$$

where $|v(q_A(t; k), \Delta_0, [\Delta])_j|$ is the j^{th} component of the robust input.

This theorem requires that α is linear with positive slope rather than an arbitrary extended class \mathcal{K}_∞ function. The proof could be extended to any \mathcal{K}_∞ function, but would generate a bound that is more difficult to compute. As we show in Sec. IX, a linear α works well. Using (85), we bound the robust input by a constant in each dimension. That is, we let

$$\begin{aligned} \mathbf{v}_j(\mathbf{q}_A(\mathbf{T}_i; \mathbf{K}), \Delta_0, [\Delta]) &= \left(\frac{\alpha_c \mathcal{E}(\sigma_M - \sigma_m)}{2} + \right. \\ &\left. + \frac{\|w_M(\ast)\| + w_M(\ast)_j}{2} \right) x_{v_j} \end{aligned} \quad (86)$$

with $w_M(\ast)$ as in Thm. 19 and x_{v_j} an indeterminate in $[-1, 1]$. Using this we let

$$\mathbf{v}(\mathbf{q}_A(\mathbf{T}_i; \mathbf{K}), \Delta_0, [\Delta]) = \bigtimes_{j=1}^{n_q} \mathbf{v}_j(\mathbf{q}_A(\mathbf{T}_i; \mathbf{K}), \Delta_0, [\Delta]). \quad (87)$$

We define the *input reachable set* for the i^{th} timestep as

$$\begin{aligned} \mathbf{u}(\mathbf{q}_A(\mathbf{T}_i; \mathbf{K}), \Delta_0, [\Delta]) &= \boldsymbol{\tau}(\mathbf{q}_A(\mathbf{T}_i; \mathbf{K}), \Delta_0) + \\ &- \mathbf{v}(\mathbf{q}_A(\mathbf{T}_i; \mathbf{K}), \Delta_0, [\Delta]). \end{aligned} \quad (88)$$

Because the robust input bound is treated as constant in each dimension in (86), when we slice the input reachable set by k , we only slice the polynomial zonotope representation of the nominal input by k , i.e.,

$$\begin{aligned} \mathbf{u}(\mathbf{q}_A(\mathbf{T}_i; k), \Delta_0, [\Delta]) &= \boldsymbol{\tau}(\mathbf{q}_A(\mathbf{T}_i; k), \Delta_0) + \\ &- \mathbf{v}(\mathbf{q}_A(\mathbf{T}_i; \mathbf{K}), \Delta_0, [\Delta]). \end{aligned} \quad (89)$$

Using these definitions and the fact that all relevant operations involving polynomial zonotopes are either exact or overapproximate, one can prove that the input reachable set contains the robust passivity-based control input:

Lemma 20 (Input PZ Conservativeness). *The input reachable set is over approximative, i.e., for each $k \in \mathbf{K}$*

$$u(q_A(t; k), \Delta_0, [\Delta]) \in \mathbf{u}(q_A(\mathbf{T}_i; k), \Delta_0, [\Delta]), \quad \forall t \in \mathbf{T}_i. \quad (90)$$

C. Constraint Generation

We now have all the components to represent the trajectory optimization constraints using polynomial zonotopes. Recall, that one can compute a conservative bound on the maximum or minimum of a polynomial zonotope by applying the \sup and \inf operators as in (14) and (15), respectively

1) *Joint Limit Constraints:* The polynomial zonotopes $\mathbf{q}_j(\mathbf{T}_i; \mathbf{K})$ and $\dot{\mathbf{q}}_j(\mathbf{T}_i; \mathbf{K})$ incorporate tracking error and overapproximate all reachable joint angles and velocities over each time step. Choosing k such that $\mathbf{q}_j(\mathbf{T}_i; k)$ and $\dot{\mathbf{q}}_j(\mathbf{T}_i; k)$ are completely contained within $[q_{j,\text{lim}}^-, q_{j,\text{lim}}^+]$ and $[\dot{q}_{j,\text{lim}}^-, \dot{q}_{j,\text{lim}}^+]$, respectively, ensures that position and velocity limits are always satisfied.

2) *Collision Avoidance Constraints:* The forward occupancy of each of the robot's links is overapproximated by $\mathbf{FO}_j(\mathbf{q}(\mathbf{T}_i; \mathbf{K}))$. The robot must never collide with obstacles, which is guaranteed by choosing k such that $\mathbf{FO}_j(\mathbf{q}(\mathbf{T}_i; k)) \cap \mathcal{O} = \emptyset$. Because the obstacles are convex polytopes (Assum. 3), one can compute a halfspace representation of obstacle O given by $A_O \in \mathbb{R}^{n_f \times 3}$ and $b_O \in \mathbb{R}^{n_f}$, where n_f is the number of faces of O . A point $p_1 \in \mathbb{R}^3$ is contained within the obstacle if and only if $A_O p_1 - b_O \leq 0$, where the inequality is taken element-wise. Therefore, p_1 lies outside the obstacle if any of the inequalities do not hold. More succinctly, $p_1 \notin O \iff \max(A_O p_1 - b_O) > 0$, where the max is taken element-wise. This implies that $\mathbf{FO}_j(\mathbf{q}(\mathbf{T}_i; k)) \cap O = \emptyset \iff \max(A_O p_1 - b_O) > 0, \forall p_1 \in \mathbf{FO}_j(\mathbf{q}(\mathbf{T}_i; k))$. The expression $A_O \mathbf{FO}_j(\mathbf{q}(\mathbf{T}_i; k)) - b_O$ yields an $n_f \times 1$ polynomial zonotope. The constraint that $\mathbf{FO}_j(\mathbf{q}(\mathbf{T}_i; k))$ does not intersect O can be written as $-\max(\inf(A_O \mathbf{FO}_j(\mathbf{q}(\mathbf{T}_i; k)) - b_O)) < 0$, where the max is taken element-wise.

3) *Input Constraints:* The input polynomial zonotope $\mathbf{u}(q_A(\mathbf{T}_i; \mathbf{K}), \Delta_0, [\Delta])$ is formed by applying (88). Importantly, the disturbances (caused by inertial parameter mismatch) and tracking error are not known at the time of planning. The input polynomial zonotopes deal with these conservatively by assuming the worst-case disturbances and tracking error. Choosing k such that $\mathbf{u}(q_A(\mathbf{T}_i; k), \Delta_0, [\Delta]) \subseteq [u_{j,\text{lim}}^-, u_{j,\text{lim}}^+]$ ensures that torque limits are not violated.

D. Trajectory Optimization

We combine these polynomial zonotope constraints within a trajectory optimization program. We seek to minimize a user-specified cost (such as reaching a desired intermediate waypoint) while satisfying each safety constraint:

$$\min_{k \in \mathbf{K}} \text{cost}(k) \quad (91)$$

$$\mathbf{q}_j(\mathbf{T}_i; k) \subseteq [q_{j,\text{lim}}^-, q_{j,\text{lim}}^+] \quad \forall i \in N_t, j \in N_q \quad (92)$$

$$\dot{\mathbf{q}}_j(\mathbf{T}_i; k) \subseteq [\dot{q}_{j,\text{lim}}^-, \dot{q}_{j,\text{lim}}^+] \quad \forall i \in N_t, j \in N_q \quad (93)$$

$$\mathbf{u}(q_A(\mathbf{T}_i; k), \Delta_0, [\Delta]) \subseteq [u_{j,\text{lim}}^-, u_{j,\text{lim}}^+] \quad \forall i \in N_t, j \in N_q \quad (94)$$

$$\mathbf{FO}_j(\mathbf{q}(\mathbf{T}_i; k)) \cap \mathcal{O} = \emptyset \quad \forall i \in N_t, j \in N_q. \quad (95)$$

Algorithm 4:

$$\{k^*\} = \text{Opt}(q_{d_0}, \dot{q}_{d_0}, \ddot{q}_{d_0}, \mathcal{O}, \text{cost}, t_p, N_t, \Delta_0, [\Delta])$$

```

1: Parfor  $i = 1 : N_t$ 
2:    $\{\mathbf{q}(\mathbf{T}_i; \mathbf{K}), \dots, \dot{\mathbf{q}}_d(\mathbf{T}_i; \mathbf{K})\} \leftarrow \text{PZ}(q_{d_0}, \dot{q}_{d_0}, \ddot{q}_{d_0})$  // Sec. VIII-A
3:    $\mathbf{q}_A(\mathbf{T}_i; \mathbf{K}) \leftarrow \{\mathbf{q}(\mathbf{T}_i; \mathbf{K}), \dots, \dot{\mathbf{q}}_d(\mathbf{T}_i; \mathbf{K})\}$  // Sec. VIII-B3
4:   // create forward occupancy reachable set //
5:    $\mathbf{FK}(\mathbf{q}(\mathbf{T}_i; \mathbf{K})) \leftarrow \text{PZFK}(\mathbf{q}(\mathbf{T}_i; \mathbf{K}))$  // Alg. 2
6:    $\mathbf{FO}(\mathbf{q}(\mathbf{T}_i; \mathbf{K})) \leftarrow (78)$ 
7:   // create input reachable set //
8:    $\boldsymbol{\tau}(q_A(\mathbf{T}_i; \mathbf{K}), \Delta_0) \leftarrow \text{PZRNEA}(q_A(\mathbf{T}_i; \mathbf{K}), \Delta_0)$  // Alg. 3
9:    $\mathbf{v}(q_A(\mathbf{T}_i; \mathbf{K}), \Delta_0, [\Delta]) \leftarrow (87)$ 
10:   $\mathbf{u}(q_A(\mathbf{T}_i; \mathbf{K}), \Delta_0, [\Delta]) \leftarrow (88)$ 
11:  // create constraints //
12:   $\text{jointCons}(\mathbf{q}(\mathbf{T}_i; \mathbf{K}), \dot{\mathbf{q}}(\mathbf{T}_i; \mathbf{K}))$  // Sec. VIII-C1
13:   $\text{collisionCons}(\mathbf{FO}(\mathbf{q}(\mathbf{T}_i; \mathbf{K})), \mathcal{O})$  // Sec. VIII-C2
14:   $\text{inputCons}(\mathbf{u}(\mathbf{T}_i; \mathbf{K}))$  // Sec. VIII-C3
15: End Parfor
16: Try:  $k^* \leftarrow \text{solve}(91) - (95)$ 
17: Catch: (if  $t_e > t_p$ ), then  $k^* = \text{NaN}$  //  $t_e$  measures the amount
    of time since  $\text{Opt}$  was called //

```

By applying Lem. 16, 17, and 20 one can prove that any feasible solution to this optimization problem can be tracked safely by the robot:

Lemma 21 (Traj. Opt. Safety). *Suppose $k \in K$ satisfies the constraints in (92)–(95), then k can be tracked for all t in T by the robot while satisfying joint and input limits and without colliding into any obstacles.*

E. ARMOUR's Online Operation

ARMOUR's planning algorithm is summarized in Alg. 4. Note in particular, that the construction and solving of the optimization problem described in lines (92)–(95) is given t_p time. If a solution is not found within that time, then the output of Alg. 4 is set to NaN. To facilitate real-time motion planning, we include the analytical constraint gradients when numerically solving the optimization problem. As described above, each constraint contains a polynomial zonotope whose coefficients correspond to the trajectory parameters and are also the decision variables of the optimization problem. Because each polynomial zonotope can be viewed as a polynomial function solely of the trajectory parameters, we can compute each constraint gradient with respect to the trajectory parameter k using the standard rules of differential calculus, i.e., the power, product, and chain rules.

Algorithm 5 summarizes the online operation of ARMOUR. ARMOUR uses the robust passivity-based controller (38) to track the trajectory parameter computed at the previous planning iteration on Line 6. While this input is being applied, ARMOUR computes the trajectory to be tracked at the next planning iteration on Line 7. By applying Cor. 11 and Lem. 21, one can prove that ARMOUR generates dynamically feasible, collision free behavior:

Lemma 22 (ARMOUR is Safe). *If q_{start} is collision free and one applies ARMOUR, as described in Algorithm 5, then the robot is collision free.*

In practice, the robust passivity-based controller on Line 6 is computed at discrete time instances at the input sampling

Algorithm 5: ARMOUR Online Planning and Control

```
1: Require:  $t_p > 0$ ,  $N_t \in \mathbb{N}$ ,  $[\Delta], \Delta_0 \in [\Delta], \mathcal{O}$ , and  $\text{cost} : K \rightarrow \mathbb{R}$ ,  
2: Initialize:  $j = 0$ ,  $t_j = 0$ , and  
    $\{k_j^*\} = \text{Opt}(q_{\text{start}}, 0, 0, \mathcal{O}, \text{cost}, t_p, N_t, \Delta_0, [\Delta])$   
3: If  $k_j^* = \text{NaN}$ , then break  
4: Loop:  
5: // Line 6 executes simultaneously with Lines 7 – 9 //  
6: // Use Thm. 10, Lem. 13, and Alg. 1 //  
   Apply  $u(q_A^j(t; k_j^*), \Delta_0, [\Delta])$  to robot for  $t \in [t_j, t_j + t_p]$   
7:  $\{k_{j+1}^*\} = \text{Opt}(q_d(t_p; k_j^*), \dot{q}_d^j(t_p; k_j^*), \ddot{q}_d^j(t_p; k_j^*), \mathcal{O},$   
    $\text{cost}, t_p, N_t, \Delta_0, [\Delta])$  // Alg. 4  
8: If  $k_{j+1}^* = \text{NaN}$ , then break  
9: Else  $t_{j+1} \leftarrow t_j + t_p$  and  $j \leftarrow j + 1$   
10: End  
11: Apply  $u(q_A^j(t; k_j^*), \Delta_0, [\Delta])$  to robot for  $t \in [t_j + t_p, t_j + t_f]$ 
```

rate requested by the robot. As we describe in Sec. IX, the input sampling rate of manipulator robots are typically a kilohertz or more [53], [54]. Fortunately, the robust passivity-based controller can be computed at that rate. However, the input applied into the robot is usually zero-order held between sampling instances. To apply Cor. 11 in this instance, one would need to show that the tracking error bound was still satisfied if the input was applied in this zero-order held fashion. Note, one could extend the results in this paper to address this additional requirement by extending the controller presented in this paper to deal with arbitrary bounded input disturbances [51, (1)]. However, this extension falls out of the scope of this paper.

IX. DEMONSTRATIONS

We demonstrate ARMOUR in simulation and on hardware using the Kinova Gen3 7 DOF robotic arm. Our code can be found online¹.

A. Implementation Details

ARMOUR is implemented in MATLAB, C++, and CUDA on a desktop with a 16 core 32 thread processor, 128 GB RAM, and Nvidia Quadro RTX 8000 GPU. Polynomial zonotopes and their arithmetic in C++/CUDA based on the CORA toolbox [55].

1) *Kinova Robot:* The Kinova Gen3 is composed of 7 revolute DOFs [53]. During the simulation evaluation, we use the Kinova arm without its gripper. We sampled a million configurations and found that the minimum and maximum eigenvalues of its mass matrix were uniformly bounded from above and below by $\sigma_M = 15.79636$ and $\sigma_m = 5.09562$, respectively. During the real-world evaluation, we use the Kinova arm with its gripper and a 2 lb dumbbell rigidly attached to the gripper. The minimum and maximum eigenvalues of its mass matrix were uniformly bounded from above and below by $\sigma_M = 18.2726$ and $\sigma_m = 8.29939$, respectively.

We consider two setups for adding uncertainty to the arm. The first case is used in simulation evaluation, which allows the mass of each link of the robot to vary by $\pm 3\%$ of its

nominal value. The inertia matrices of each link vary accordingly. We refer to this setup as the “standard” set of inertial parameters, denoted by $[\Delta]$. The second case is used in real-world evaluation, which rigidly attaches a 2 lb dumbbell to the arm’s end effector. The geometry of the dumbbell is considered when checking for collisions. We treat the dumbbell’s inertia as a point mass located at its centroid, and allow its mass to vary by $\pm 3\%$, without varying the rest of the arm’s parameters. We call this the “dumbbell” set of inertial parameters, denoted by $[\Delta]_{\text{db}}$.

2) *Planning Times and Trajectories:* We let $t_p = 0.5\text{s}$, and $t_f = 1\text{s}$. As in Ex. 15, we represent our desired trajectories using a degree 5 Bernstein polynomial and let $\eta_{j,2} = q_{d,j_0}$ and $\eta_{j,1} = \frac{\pi}{48}$.

3) *Controller:* For the nominal passivity-based controller we set $K_r = 5I_7$, where I_7 is a 7×7 identity matrix. During our experiments, we were able to compute the passivity-based control input at approximately 15kHz . However, the software for the arm only required a control update at 1kHz .

For the robust controller, several additional parameters must be specified. As in Thm. 19, we set $\alpha(y) = y$. We let the Lyapunov function threshold be $V_M = 1 \times 10^{-2}$. When we run the experiment in simulation, we do it without the gripper and the uniform bound is $\varepsilon = \sqrt{\frac{2V_M}{\sigma_m}} = \sqrt{\frac{2 \times 1 \times 10^{-2}}{5.09562}} \approx 0.062649$. Plugging into the position (55) and velocity (56) bounds yields $\varepsilon_{p,j} \approx 0.01253$ rad and $\varepsilon_v \approx 0.02506$ rad/s.

4) *High-level Planners:* In each planning iteration, ARMOUR minimizes a user-specified cost subject to the constraints detailed in Sec. VIII. This work formulates the cost as minimizing the distance between $q_d(t_f; k)$ and an intermediate waypoint q_{des} . We use high-level planners to construct these intermediate waypoints, which form a rough path to the global goal. ARMOUR is independent of the high-level planner, which is only used for the cost function. ARMOUR enforces safety even if the high-level planner’s waypoints are in collision or not dynamically feasible. In the majority of simulations presented here, we use a straight line high-level planner that generates waypoints along a straight line (in configuration space) between the start and goal configurations. For some scenarios (detailed below), we also test an RRT* [7] that only ensures the robot’s end effector is collision free.

5) *Comparisons:* We compare ARMOUR to a previous version of the method ARMTD [3] by running the algorithms on identical random worlds with the same high-level planner. We also compare ARMOUR to CHOMP [9] (run via MoveIt [56]) as was done previously with ARMTD. Although CHOMP is not a receding-horizon planner, it provides a useful baseline for measuring the difficulty of the scenarios encountered by ARMOUR. **ARMTD and CHOMP are given the true inertial parameters, but ARMOUR is not given the true inertial parameters.** This means that ARMTD and CHOMP can perfectly track trajectories that they compute while ARMOUR may not be able to, which should give ARMTD and CHOMP a considerable advantage when compared to ARMOUR.

6) *Algorithm Implementation:* We solve ARMOUR’s trajectory optimization using Ipopt [57]. We provide analytic gradients to the optimization solver to speed computation.

¹<https://github.com/roahmlab/armour>

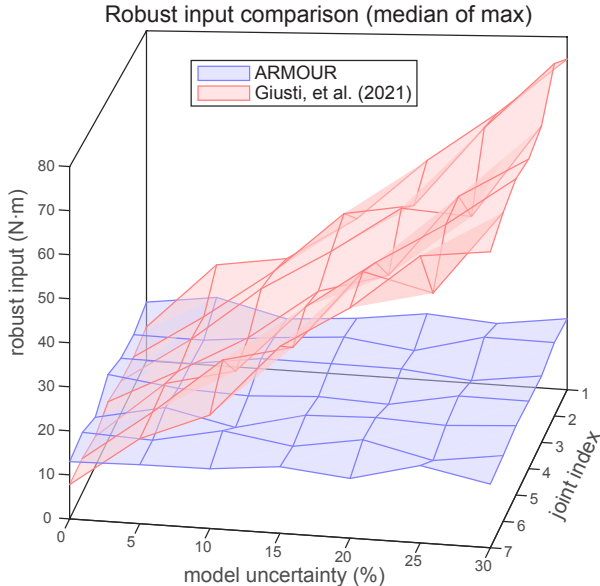


Fig. 5. Robust input comparison. This figure compares ARMOUR’s robust input (52) to that of [37, Theorem 2] across each of the robot’s joints. The uncertainty in the mass and the inertia of each link was varied between 0-30%. Compared to [51], ARMOUR’s robust input is far less sensitive to increasing model uncertainty.

B. Robust Controller Comparison

We compare the performance of our controller’s robust input (52) to that of [51] under different model uncertainties². In Def. 6 and Thm. 10, we construct the desired trajectories such that the tracking error is always bounded. Within our planning framework, this ensures that the robot stays within the reachable set despite model uncertainty. However, our controller can be applied more generally without assumptions on the initial state of the robot.

In this experiment, we perturb the initial state of the desired trajectory such that the tracking error is not always guaranteed to be inside the ultimate bound. This allows us to compare the magnitude of the robust input required to correct the tracking error to within the ultimate bound. We compared the robust inputs across 7 different model uncertainties, ranging from 0% to 30% in the mass and inertia of each link. The parameters of the two controllers are chosen such that their ultimate bounds are the same. We randomized the perturbation added to the initial state of all 7 joints. The magnitude of the perturbation added to the initial position and initial velocity are 4.5 degrees and 9 degrees/second, respectively. For each model uncertainty, we perform 100 experiments where each controller tracks a desired trajectory for 2.5 seconds after the initial state of the robot is randomly perturbed. Note that the ultimate bound was usually reached within 1.5 seconds for either controller. We then take the maximum robust input of each experiment and plot the median over all experiments. As shown in Fig. 5, our controller applies a smaller robust input to achieve the same ultimate tracking performance.

²Note for a comparison between the input bounds derived from our robust input and that of [51], please see <https://github.com/roahmlab/armour/blob/main/assets/TRO-Armour-Appendix-F.pdf>

TABLE II
Results for the 100 Random Obstacles simulations. ARMTD and ARMOUR use straight-line (SL) HLPs.

Random Obstacles	% goals	% crashes
ARMTD + SL + Δ_0	72	0
CHOMP + Δ_0	87	13
(ours) ARMOUR + SL + $[\Delta]$	92	0

C. Simulation

1) *Setup*: As in [3], we test ARMOUR on two sets of scenes. The first set, Random Obstacles, shows that ARMOUR can handle arbitrary tasks. This set contains 100 tasks with random (but collision-free) start and goal configurations, and random box-shaped obstacles. Obstacle side lengths vary from 1 to 50 cm, with 10 scenes for each $n_O = 13, 16, \dots, 37, 40$. The second set, Hard Scenarios, shows that ARMOUR guarantees safety where CHOMP converges to an unsafe trajectory. There are seven tasks in the Hard Scenarios set shown in Fig. 6. For both these sets of scenes, ARMOUR uses the “standard” inertial parameters $[\Delta]$ with 3% uncertainty in each link’s mass.

In all tests using the Random Obstacles scenario, the straight line high-level planner is used. For the Hard Scenarios set, we also present results using the RRT*.

2) *Results*: Table II (Random Obstacles) presents ARMOUR (with a straight line high-level planner) in comparison to ARMTD and CHOMP as in [3]. ARMOUR reached 92/100 goals and had 0/100 crashes, meaning ARMOUR safely stopped in 8/100 scenes without finding a new trajectory. ARMOUR takes 364.9ms on average per planning iteration. Note that ARMOUR actually outperforms ARMTD using the same high-level planner despite dealing with uncertainty in the inertial parameters $[\Delta]$. This is likely due to the updated polynomial zonotope formulation of the robot’s forward occupancy. These sets now more tightly envelope the actual reachable set of the robot, allowing for closer maneuvering around obstacles. We note that CHOMP always finds a dynamically feasible trajectory, but not necessarily a collision-free one, as demonstrated by the 13/100 crashes. In practice, an external collision-checker can be used to verify that these trajectories are collision free before commanding them on the robot, but we note that CHOMP itself does not provide this guarantee.

Table III presents results for the Hard Scenarios. With the straight line high-level planner, ARMOUR is unable to complete any tasks but also has no collisions. With the RRT* high-level planner, ARMOUR successfully completes 6/7 scenarios and safely stops in the remaining scenario. This improves on the results for ARMTD with the same high-level planner, which completed 5/7 scenarios.

D. Hardware

Finally, we applied ARMOUR to perform real-time control and planning in the real-world. using the Kinova Gen3 robot while it holds a dumbbell. A video showing a hardware demonstration of ARMOUR safely controlling the Kinova Gen3 robot is available online³. This experiment illustrates that

³<https://youtu.be/-WtxxQyoxGo?si=W2RaziwRLMosZ23L>

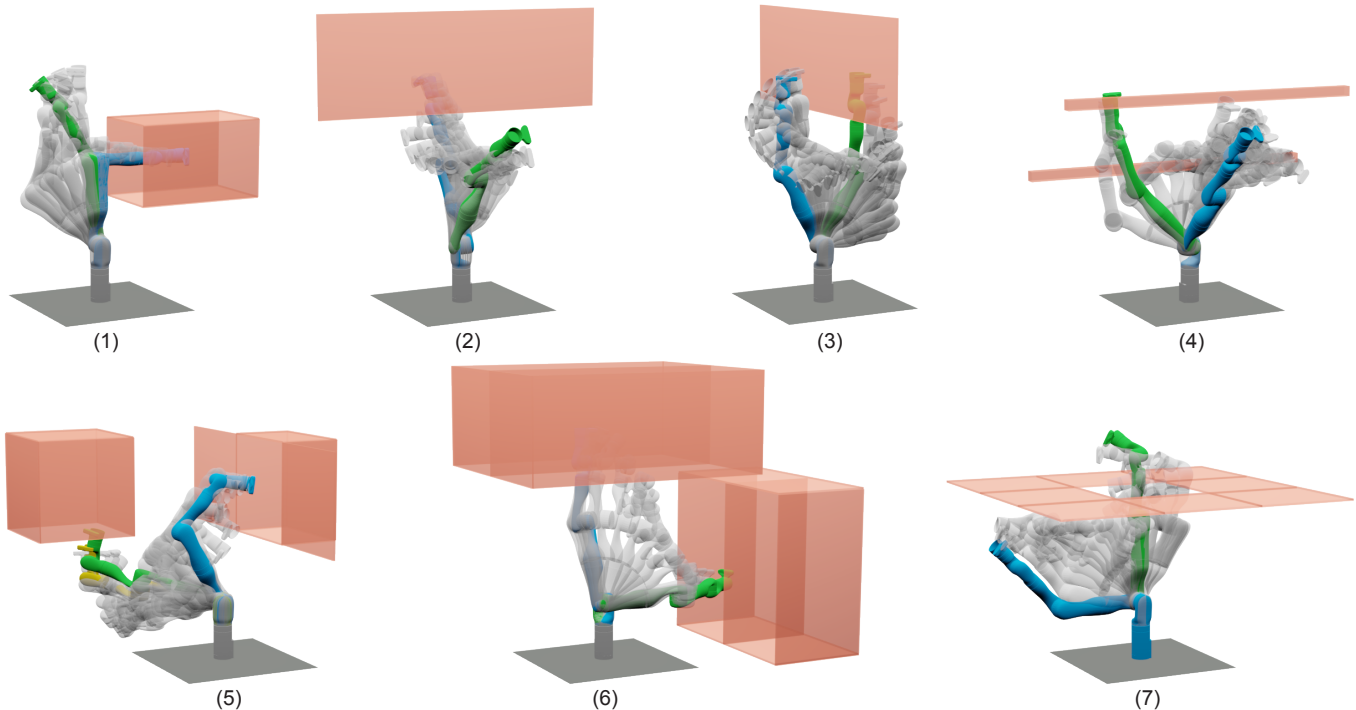


Fig. 6. The set of seven Hard Scenarios (number in the top left), with start pose shown in blue and goal pose shown in green. There are seven tasks in the Hard Scenarios set: (1) from inside to outside of a box, (2-3) from one side of a wall to another, (4) between two horizontal posts, (5) from a sink to a cupboard, (6) from one set of shelves to another, (7) through a small window. Note that ARMOUR fails to reach the goal in scenario (5) and the final pose is shown in yellow.

TABLE III

Results for the seven Hard Scenario simulations. ARMTD and ARMOUR use straight-line (SL) and RRT* HLPs. The entries are “O” for task completed, “C” for a crash, or “S” for stopping safely without reaching the goal.

Hard Scenarios	1	2	3	4	5	6	7
CHOMP + Δ_0	C	C	C	C	C	C	C
ARMTD + RRT* + Δ_0	O	O	O	S	S	O	O
(ours) ARMOUR + SL + $[\Delta]$	S	S	S	S	S	S	S
(ours) ARMOUR + RRT* + $[\Delta]$	O	O	O	O	S	O	O

ARMOUR can operate safely in real-time despite modeling uncertainty.

X. CONCLUSION

We present ARMOUR, a real-time planning and control framework with strict safety guarantees for manipulators with set-based uncertainty in their inertial parameters. A robust control formulation (Thm. 10) provides uniform bounds on the worst-case tracking error possible when following desired trajectories. The PZRNEA algorithm (Alg. 3) enables ARMOUR to compute sets of possible inputs required to track any desired trajectory, including tracking error. Polynomial zonotope arithmetic also enables the formulation of continuous-time collision-avoidance constraints. Strict joint limit, torque limit, and collision-avoidance constraints are implemented within a nonlinear program that is solved at every iteration of ARMOUR’s receding-horizon planning scheme. By designing the inclusion of a fail-safe braking maneuver in every desired

trajectory, ARMOUR guarantees the safe operation of the robotic arm for all time.

REFERENCES

- [1] A. De Luca and L. Ferrajoli, “A modified newton-euler method for dynamic computations in robot fault detection and control,” in *2009 IEEE International Conference on Robotics and Automation*, 2009, pp. 3359–3364.
- [2] N. Kochdumper and M. Althoff, “Sparse polynomial zonotopes: A novel set representation for reachability analysis,” *IEEE Transactions on Automatic Control*, vol. 66, no. 9, pp. 4043–4058, 2020.
- [3] P. Holmes, S. Kousik, B. Zhang, *et al.*, “Reachable Sets for Safe, Real-Time Manipulator Trajectory Design,” in *Proceedings of Robotics: Science and Systems*, Corvallis, Oregon, USA, Jul. 2020.
- [4] E. Yoshida, I. Belousov, C. Esteves, and J.-P. Laumond, “Humanoid motion planning for dynamic tasks,” in *5th IEEE-RAS International Conference on Humanoid Robots, 2005.*, IEEE, 2005, pp. 1–6.
- [5] H. Dai, A. Valenzuela, and R. Tedrake, “Whole-body motion planning with centroidal dynamics and full kinematics,” in *2014 IEEE-RAS International Conference on Humanoid Robots*, IEEE, 2014, pp. 295–302.
- [6] S. Kousik, S. Vaskov, F. Bu, M. Johnson-Roberson, and R. Vasudevan, “Bridging the gap between safety and real-time performance in receding-horizon trajectory design for mobile robots,” *The International Journal of Robotics Research*, vol. 39, no. 12, pp. 1419–1469, 2020.
- [7] S. Karaman and E. Frazzoli, “Sampling-based algorithms for optimal motion planning,” *The international journal of robotics research*, vol. 30, no. 7, pp. 846–894, 2011.
- [8] L. E. Kavraki, P. Svestka, J.-C. Latombe, and M. H. Overmars, “Probabilistic roadmaps for path planning in high-dimensional configuration spaces,” *IEEE transactions on Robotics and Automation*, vol. 12, no. 4, pp. 566–580, 1996.
- [9] M. Zucker, N. Ratliff, A. D. Dragan, *et al.*, “Chomp: Covariant hamiltonian optimization for motion planning,” *The International Journal of Robotics Research*, vol. 32, no. 9–10, pp. 1164–1193, 2013.

- [10] J. Schulman, Y. Duan, J. Ho, *et al.*, “Motion planning with sequential convex optimization and convex collision checking,” *The International Journal of Robotics Research*, vol. 33, no. 9, pp. 1251–1270, 2014.
- [11] M. Elbanhawi and M. Simic, “Sampling-based robot motion planning: A review,” *Ieee access*, vol. 2, pp. 56–77, 2014.
- [12] Z. Kingston, M. Moll, and L. E. Kavraki, “Sampling-based methods for motion planning with constraints,” *Annual review of control, robotics, and autonomous systems*, vol. 1, pp. 159–185, 2018.
- [13] M. Kalakrishnan, S. Chitta, E. Theodorou, P. Pastor, and S. Schaal, “Stomp: Stochastic trajectory optimization for motion planning,” in *2011 IEEE international conference on robotics and automation*, IEEE, 2011, pp. 4569–4574.
- [14] L. Jaillet and J. M. Porta, “Path planning under kinematic constraints by rapidly exploring manifolds,” *IEEE Transactions on Robotics*, vol. 29, no. 1, pp. 105–117, 2012.
- [15] J. M. Porta, L. Jaillet, and O. Bohigas, “Randomized path planning on manifolds based on higher-dimensional continuation,” *The International Journal of Robotics Research*, vol. 31, no. 2, pp. 201–215, 2012.
- [16] I. A. Şucan and S. Chitta, “Motion planning with constraints using configuration space approximations,” in *2012 IEEE/RSJ International Conference on Intelligent Robots and Systems*, IEEE, 2012, pp. 1904–1910.
- [17] S. M. Lavalle and R. Sharma, “On motion planning in changing, partially predictable environments,” *The International Journal of Robotics Research*, vol. 16, no. 6, pp. 775–805, 1997.
- [18] D. Berenson, S. S. Srinivasa, D. Ferguson, and J. J. Kuffner, “Manipulation planning on constraint manifolds,” in *2009 IEEE international conference on robotics and automation*, IEEE, 2009, pp. 625–632.
- [19] D. Beckert, A. Pereira, and M. Althoff, “Online verification of multiple safety criteria for a robot trajectory,” in *2017 IEEE 56th Annual Conference on Decision and Control (CDC)*, IEEE, 2017, pp. 6454–6461.
- [20] L. Scalera, R. Vidoni, and A. Giusti, “Optimal scaling of dynamic safety zones for collaborative robotics,” in *2021 IEEE International Conference on Robotics and Automation (ICRA)*, IEEE, 2021, pp. 3822–3828.
- [21] L. Scalera, A. Giusti, R. Vidoni, and A. Gaspardo, “Online planning of path-consistent stop trajectories for collaborative robotics,” in *The International Conference of IFToMM ITALY*, Springer, 2022, pp. 693–701.
- [22] J. J. Kuffner, S. Kagami, K. Nishiwaki, M. Inaba, and H. Inoue, “Dynamically-stable motion planning for humanoid robots,” *Autonomous robots*, vol. 12, no. 1, pp. 105–118, 2002.
- [23] F. Kanehiro, W. Suleiman, F. Lamiroux, E. Yoshida, and J.-P. Laumond, “Integrating dynamics into motion planning for humanoid robots,” in *2008 IEEE/RSJ International Conference on Intelligent Robots and Systems*, IEEE, 2008, pp. 660–667.
- [24] Y. Han, R. Li, and G. S. Chirikjian, “Can i lift it? humanoid robot reasoning about the feasibility of lifting a heavy box with unknown physical properties,” in *2020 IEEE/RSJ International Conference on Intelligent Robots and Systems (IROS)*, IEEE, 2020, pp. 3877–3883.
- [25] N. D. Ratliff, J. Issac, D. Kappler, S. Birchfield, and D. Fox, “Riemannian motion policies,” *arXiv preprint arXiv:1801.02854*, 2018.
- [26] A. Bylard, R. Bonalli, and M. Pavone, “Composable geometric motion policies using multi-task pullback bundle dynamical systems,” *arXiv e-prints*, arXiv–2101, 2021.
- [27] C. Abdallah, D. M. Dawson, P. Dorato, and M. Jamshidi, “Survey of robust control for rigid robots,” *IEEE Control Systems Magazine*, vol. 11, no. 2, pp. 24–30, 1991.
- [28] H. Sage, M. De Mathelin, and E. Ostertag, “Robust control of robot manipulators: A survey,” *International Journal of control*, vol. 72, no. 16, pp. 1498–1522, 1999.
- [29] J.-J. Slotine and S. S. Sastry, “Tracking control of non-linear systems using sliding surfaces, with application to robot manipulators,” *International journal of control*, vol. 38, no. 2, pp. 465–492, 1983.
- [30] J.-J. E. Slotine, “The robust control of robot manipulators,” *The International Journal of Robotics Research*, vol. 4, no. 2, pp. 49–64, 1985.
- [31] S. Islam and X. P. Liu, “Robust sliding mode control for robot manipulators,” *IEEE Transactions on industrial electronics*, vol. 58, no. 6, pp. 2444–2453, 2010.
- [32] M. B. R. Neila and D. Tarak, “Adaptive terminal sliding mode control for rigid robotic manipulators,” *International Journal of Automation and Computing*, vol. 8, no. 2, pp. 215–220, 2011.
- [33] J. Baek, M. Jin, and S. Han, “A new adaptive sliding-mode control scheme for application to robot manipulators,” *IEEE Transactions on industrial electronics*, vol. 63, no. 6, pp. 3628–3637, 2016.
- [34] M. Zhu, L. Ye, and X. Ma, “Estimation-based quadratic iterative learning control for trajectory tracking of robotic manipulator with uncertain parameters,” *IEEE Access*, vol. 8, pp. 43 122–43 133, 2020.
- [35] A. Giusti and M. Althoff, “Efficient computation of interval-arithmetic-based robust controllers for rigid robots,” in *2017 First IEEE International Conference on Robotic Computing (IRC)*, IEEE, 2017, pp. 129–135.
- [36] M. Wagner, S. Liu, A. Giusti, and M. Althoff, “Interval-arithmetic-based trajectory scaling and collision detection for robots with uncertain dynamics,” in *2018 Second IEEE International Conference on Robotic Computing (IRC)*, IEEE, 2018, pp. 41–48.
- [37] A. Giusti, S. B. Liu, and M. Althoff, “Interval-arithmetic-based robust control of fully actuated mechanical systems,” *IEEE Transactions on Control Systems Technology*, Oct. 2021.
- [38] S. Malan, M. Milanese, and M. Taragna, “Robust analysis and design of control systems using interval arithmetic,” *Automatica*, vol. 33, no. 7, pp. 1363–1372, 1997.
- [39] Y. Smagina and I. Brewer, “Using interval arithmetic for robust state feedback design,” *Systems & Control Letters*, vol. 46, no. 3, pp. 187–194, 2002.
- [40] L. Jaulin, “Nonlinear bounded-error state estimation of continuous-time systems,” *Automatica*, vol. 38, no. 6, pp. 1079–1082, 2002.
- [41] J. M. Bravo, D. Limón, T. Alamo, and E. F. Camacho, “On the computation of invariant sets for constrained nonlinear systems: An interval arithmetic approach,” *Automatica*, vol. 41, no. 9, pp. 1583–1589, 2005.
- [42] T. Hickey, Q. Ju, and M. H. Van Emden, “Interval arithmetic: From principles to implementation,” *Journal of the ACM (JACM)*, vol. 48, no. 5, pp. 1038–1068, 2001.
- [43] M. Althoff, “Reachability analysis and its application to the safety assessment of autonomous cars,” Ph.D. dissertation, Technische Universität München, 2010.
- [44] M. Althoff, “Reachability analysis of nonlinear systems using conservative polynomialization and non-convex sets,” in *Proceedings of the 16th international conference on Hybrid systems: computation and control*, 2013, pp. 173–182.
- [45] T. M. Apostol, *Calculus, Volume 1*. John Wiley & Sons, 1991.
- [46] M. Spong, S. Hutchinson, and M. Vidyasagar, “Robot modeling and control,” 2005.
- [47] L. J. Guibas, A. Nguyen, and L. Zhang, “Zonotopes as bounding volumes,” in *Proceedings of the fourteenth annual ACM-SIAM symposium on Discrete algorithms*, Society for Industrial and Applied Mathematics, 2003, pp. 803–812.
- [48] S. Vaskov, S. Kousik, H. Larson, *et al.*, “Towards provably not-at-fault control of autonomous robots in arbitrary dynamic environments,” in *Proceedings of Robotics: Science and Systems*, Freiburg/Breisgau, Germany, Jun. 2019.
- [49] S. Kousik, P. Holmes, and R. Vasudevan, “Safe, aggressive quadrotor flight via reachability-based trajectory design,” in *Dynamic Systems and Control Conference*, American Society of Mechanical Engineers, vol. 59162, 2019, V003T19A010.
- [50] J. Liu, Y. Shao, L. Lyburner, *et al.*, “Refine: Reachability-based trajectory design using robust feedback linearization and zonotopes,” *arXiv preprint arXiv:2211.11997*, 2022.
- [51] A. Giusti and M. Althoff, “Ultimate robust performance control of rigid robot manipulators using interval arithmetic,” in *2016 American Control Conference (ACC)*, 2016, pp. 2995–3001.
- [52] C. C. de Wit, B. Siciliano, and G. Bastin, *Theory of robot control*. Springer Science & Business Media, 2012.
- [53] Kinova, *User Guide - KINOVA Gen3 Ultra lightweight robot*. 2022.
- [54] Franka, *User Guide - PANDA - DATASHEET*. 2019.
- [55] M. Althoff, “An Introduction to CORA 2015,” in *Proc. of the Workshop on Applied Verification for Continuous and Hybrid Systems*, 2015.
- [56] D. Coleman, I. A. Sucas, S. Chitta, and N. Correll, “Reducing the Barrier to Entry of Complex Robotic Software: a MoveIt! Case Study,” *CoRR*, vol. abs/1404.3785, 2014.
- [57] A. Wächter and L. Biegler, “On the implementation of an interior-point filter line-search algorithm for large-scale nonlinear programming,” *Mathematical programming*, vol. 106, pp. 25–57, Mar. 2006.
- [58] R. Konda, A. D. Ames, and S. Coogan, “Characterizing safety: Minimal control barrier functions from scalar comparison systems,” *IEEE Control Systems Letters*, vol. 5, no. 2, pp. 523–528, 2020.

- [59] B. Siciliano, L. Sciacivco, L. Villani, and G. Oriolo, "Modelling, planning and control," *Advanced Textbooks in Control and Signal Processing*. Springer, 2009.

APPENDIX A
PROOF OF THM. 10

Proof. Let $h(q_A(t), \Delta) = -V(q_A(t), \Delta) + V_M$. This proof shows that h is a minimal Control Barrier Function (CBF) under the input (52) [58, Def. 3]. With this property and if (52) is continuous with respect to its first argument, then all zero super-level sets of h , defined as $H = \{q_A(t) \mid h(q_A(t), \Delta) \geq 0\}$, are forward invariant [58, Thm. 4]. If H is forward invariant, this proves the bound on $r(t)$. To see this, note the trajectory starts in H , and as a result will remain in H . Next, note that $V(q_A(t), \Delta) \leq V_M, \forall q_A(t) \in H$. By applying Ass. 9:

$$\frac{1}{2} \sigma_m \|r(t)\|^2 \leq \frac{1}{2} r(t)^\top M(q(t), \Delta) r(t) = V(q_A(t), \Delta). \quad (96)$$

Therefore, $\|r(t)\| \leq \varepsilon, \forall q_A(t) \in H$. So, we show that h is a minimal control barrier function and (52) is continuous.

h is a minimal CBF: Recall that the manipulator dynamics are control affine [46, (6.61)]. To prove that h is a minimal control barrier function, we need to prove that under the robust control input:

$$\dot{h}(q_A(t), \Delta) \geq -\alpha(h(q_A(t), \Delta)). \quad (97)$$

To apply [58, Def. 3], α must be a minimal function. Any extended class \mathcal{K}_∞ function is a minimal one [58, Case 2, Thm. 2]. As we show below, \dot{h} is a function of Δ, Δ_0 , and $[\Delta]$. These dependencies are clear in context, so we suppress them.

We make several observations: V is positive definite because $M(q(t), \Delta)$ is positive definite. Next, $N(q(t), \dot{q}(t), \Delta) = \dot{M}(q(t), \Delta) - 2C(q(t), \dot{q}(t), \Delta)$ is skew-symmetric [59, Ch. 7]:

$$x^\top N(q(t), \dot{q}(t), \Delta) x = 0, \quad \forall x \in \mathbb{R}^{n_q}. \quad (98)$$

Taking the time derivative of $h(q_A(t), \Delta)$, substituting (44), and taking advantage of (98), yields

$$\begin{aligned} \dot{h}(q_A(t)) &= -r(t)^\top v(q_A(t), \Delta_0, [\Delta]) + \\ &\quad - r(t)^\top w(q_A(t), \Delta_0, \Delta), \end{aligned} \quad (99)$$

\dot{h} is a function of Δ, Δ_0 , and $[\Delta]$, but we have suppressed these dependencies. Using this result, (97) becomes

$$\begin{aligned} -r(t)^\top v(q_A(t), \Delta_0, [\Delta]) + \\ - r(t)^\top w(q_A(t), \Delta_0, \Delta) \geq -\alpha(h(q_A(t), \Delta)). \end{aligned} \quad (100)$$

Our task is to choose v so that (100) is always satisfied.

By Lem. 8 and (50), $|r(t)|^\top w_M(q_A(t), \Delta_0, [\Delta]) \geq r(t)^\top w(q_A(t), \Delta_0, \Delta)$, so we rearrange (100) to obtain:

$$\begin{aligned} -r(t)^\top v(q_A(t), \Delta_0, [\Delta]) \geq -\alpha(h(q_A(t), \Delta)) + \\ + |r(t)|^\top w_M(q_A(t), \Delta_0, [\Delta]), \end{aligned} \quad (101)$$

whose satisfaction guarantees that (100) is satisfied. The left hand side expression is maximized when $v(q_A(t), \Delta_0, [\Delta])$ points in the $-\frac{r(t)}{\|r(t)\|}$ direction. Choosing $v(q_A(t), \Delta_0, [\Delta]) = -\gamma(q_A(t), \Delta_0, [\Delta]) \frac{r(t)}{\|r(t)\|}$, where $\gamma(q_A(t), \Delta_0, [\Delta]) \geq 0$, yields

$$\gamma(q_A(t), \Delta_0, [\Delta]) \geq \frac{-\alpha(h(q_A(t), \Delta)) + |r(t)|^\top w_M(q_A(t), \Delta_0, [\Delta])}{\|r(t)\|}. \quad (102)$$

Simultaneously, choosing $\gamma(q_A(t), \Delta_0, [\Delta]) \geq 0$ while satisfying the previous equation ensures that $h(q_A(t), \Delta)$ is a minimal CBF. Computing this γ requires $h(q_A(t), \Delta)$. Because we do not know Δ , we can not compute $h(q_A(t), \Delta)$. Instead, we bound $h(q_A(t), \Delta)$ over the range of inertial parameters. $\underline{h}(q_A(t), [\Delta])$ as in (49) lower bounds $h(q_A(t), \Delta)$. The inequality $\underline{h}(q_A(t), [\Delta]) \leq h(q_A(t), \Delta)$ implies that $-\alpha(\underline{h}(q_A(t), [\Delta])) \geq -\alpha(h(q_A(t), \Delta))$, so choosing $\gamma(q_A(t), \Delta_0, [\Delta]) \geq 0$ and

$$\gamma(q_A(t), \Delta_0, [\Delta]) \geq \frac{-\alpha(\underline{h}(q_A(t), [\Delta])) + |r(t)|^\top w_M(q_A(t), \Delta_0, [\Delta])}{\|r(t)\|} \quad (103)$$

ensures that (97) is satisfied and h is a minimal CBF.

(52) is continuous: (52) could only be discontinuous when $\|r(t)\| = 0$. We prove that for all points in a neighborhood of the point $\|r(t)\| = 0$, $\gamma(q_A(t), \Delta_0, [\Delta]) = 0$ where Δ_0 and $[\Delta]$ are held fixed.

Recall from Ass. 9 that there exists $\sigma_M > 0$ such that

$$-\frac{1}{2} r(t)^\top M(q(t), \Delta) r(t) \geq -\frac{1}{2} \sigma_M \|r(t)\|^2 \quad (104)$$

for all $\Delta \in [\Delta]$ and $q(t) \in \mathcal{Q}$. Next, there exists $r_M \geq 0$ such that for all $r(t)$ with $\|r(t)\| \leq r_M$, we have $-\frac{1}{2} \sigma_M \|r(t)\|^2 + V_M > 0$. This implies that there exists some $\zeta > 0$ such that $\underline{h}(q_A(t), [\Delta]) > \zeta$ for all $q_A(t)$ with $\|r(t)\| \leq r_M$. Because α is an extended class \mathcal{K}_∞ function, this implies that

$$\begin{aligned} \frac{-\alpha(\underline{h}(q_A(t), [\Delta]))}{\|r(t)\|} + \frac{|r(t)|^\top w_M(q_A(t), \Delta_0, [\Delta])}{\|r(t)\|} < \frac{-\alpha(\zeta)}{\|r(t)\|} + \\ + \|w_M(q_A(t), \Delta_0, [\Delta])\|, \end{aligned} \quad (105)$$

where we have used the fact that $|r(t)|^\top w_M(q_A(t), \Delta_0, [\Delta]) \leq \|r(t)\| \|w_M(q_A(t), \Delta_0, [\Delta])\|$. Because $\alpha(\zeta) > 0$, the previous inequality implies $\frac{-\alpha(\underline{h}(q_A(t), [\Delta]))}{\|r(t)\|} + \|w_M(q_A(t), \Delta_0, [\Delta])\| \rightarrow -\infty$ as $\|r(t)\| \rightarrow 0$. So, $\gamma(q_A(t), \Delta_0, [\Delta]) = 0, \forall r(t)$ with $\|r(t)\| \leq r_M$. \square

APPENDIX B
PROOF OF COR. 11

Proof. Rearranging (45), we get $\dot{e}(t) = -K_r e(t) + r(t)$. K_r is diagonal, so this defines n_q first-order linear systems where we treat r as an input. The solution of the j^{th} system is

$$e_j(t) = \int_0^t \exp(-K_{r,j}(t-s)) r_j(s) ds. \quad (106)$$

because by hypothesis $e_j(0) = 0$. Using $|r_j(t)| \leq \varepsilon$, we obtain $|e_j(t)| \leq |\exp(-K_{r,j} t) \varepsilon \int_0^t \exp(K_{r,j} s) ds|$. By solving the integral and noticing that $\exp(-K_{r,j} t) \in [0, 1], \forall t \geq 0$, we get the result. The bound on the velocity error follows by using the position error bound, (45), and the triangle inequality. \square

APPENDIX C
PROOF OF LEM. 13

Proof. Because IRNEA replaces all operations over the inertial parameters in RNEA with interval arithmetic equivalents, $\text{RNEA}(q_A(t), \Delta_0, a_0^0) \in \text{IRNEA}(q_A(t), [\Delta], a_0^0)$ for $\Delta_0 \in [\Delta]$. So, $w(q_A(t), \Delta_0, \Delta) \in [w(q_A(t), \Delta_0, [\Delta])]$ and (50) follows.

The norm, max, and absolute value are all continuous functions, so if we prove that $\inf([w(q_A(t), \Delta_0, [\Delta])])$ and $\sup([w(q_A(t), \Delta_0, [\Delta])])$ are continuous in their first argument, then w_M is continuous in its first argument. To prove that, note that $q_A(t)$ is a vector rather than interval argument to IRNEA and is used to generate a homogeneous transformation matrix, which is a continuous function of $q_A(t)$. Because all operations in IRNEA are either interval additions, subtractions, or matrix multiplications of the interval inertia parameters with the homogeneous transformation matrix or the velocity/acceleration vectors in $q_A(t)$, the lower or upper bound of the interval output to IRNEA is a continuous function of $q_A(t)$.

To prove the desired result for \underline{h} , note that if we use $q_R(t)$ in place of $q_A(t)$, then when we apply (37), we have $\dot{q}_a(t) = 0$ and $\ddot{q}_a(t) = r(t)$. Because IRNEA is computing an interval version of (39) and is using interval arithmetic, $M(q(t), \Delta_0)r(t) \in \text{IRNEA}(q_R(t), [\Delta], 0)$ for $\Delta_0 \in [\Delta]$. Therefore by applying the properties of interval arithmetic, the \underline{h} defined as in (63) satisfies (49). The continuity of \underline{h} in its first argument follows by applying the same argument as above. \square

APPENDIX D LEMMA 23

The following lemma is utilized in the proof of Thm. 19.

Lemma 23. *Given vectors $a, b \in \mathbb{R}^{n_q}$ of unit norm $\|a\| = \|b\| = 1$, consider the optimization problem $\max\{f(c) \mid c \in \mathbb{R}^{n_q}, \|c\| = 1\}$, where $f(c) = (a^\top c)(b^\top c)$. At the optimal solution c^* , the cost $f(c^*) = \frac{1+a^\top b}{2}$.*

Proof. $(a^\top c - b^\top c)^2 \geq 0$, so $(a^\top c)^2 - 2(a^\top c)(b^\top c) + (b^\top c)^2 \geq 0$. Adding $4(a^\top c)(b^\top c)$ to both sides, we get $(a^\top c + b^\top c)^2 \geq 4(a^\top c)(b^\top c)$. Therefore $f(c) \leq \frac{(a^\top c + b^\top c)^2}{4}$. Note that if $a^\top c = b^\top c$, then $f(c) = \frac{(a^\top c + b^\top c)^2}{4}$. Using the distributive property on $f(c) \leq \frac{(a^\top c + b^\top c)^2}{4}$ gives $f(c) \leq \frac{((a+b)^\top c)^2}{4}$. The right hand side is maximized when c points in the $a+b$ direction, so we choose $c^* = \frac{(a+b)}{\|a+b\|}$. Plugging in, we obtain $f(c^*) \leq \frac{((a+b)^\top \frac{(a+b)}{\|a+b\|})^2}{4}$. Note that $\|a+b\|^2 = (a+b)^\top (a+b)$, and therefore $f(c^*) \leq \frac{((a+b)^\top (a+b))^2}{4(a+b)^\top (a+b)}$. Cancelling terms, multiplying, and using the fact that $a^\top a = b^\top b = 1$, we obtain $f(c^*) \leq \frac{1+a^\top b}{2}$. Finally, note that $a^\top c^* = b^\top c^* = \frac{1+a^\top b}{\|a+b\|}$, and thus $f(c^*) = \frac{(a^\top c^* + b^\top c^*)^2}{4}$ and we have the desired result. \square

APPENDIX E PROOF OF THM. 19

Proof. For notational convenience, we drop the dependence on k in q_A and r . If 0 achieves the maximum in the RHS of the expression defining γ (i.e., (53)), then $\gamma(q_A(t; k), \Delta_0, [\Delta]) = 0$ and (85) holds trivially. Therefore, we apply (52) and bound:

$$\begin{aligned} |v(q_A(t), \Delta_0, [\Delta])_j| &\leq \frac{-\alpha(\underline{h}(q_A(t), [\Delta]))}{\|r(t)\|} \frac{|r(t)_j|}{\|r(t)\|} + \\ &+ \frac{|r(t)^\top w_M(q_A(t), \Delta_0, [\Delta])|}{\|r(t)\|} \frac{|r(t)_j|}{\|r(t)\|}. \end{aligned} \quad (107)$$

In the RHS of the above inequality, note that the first term is negative when $\underline{h}(q_A(t), [\Delta]) > 0$, and that the second term is always positive (because all elements of $w_M(q_A(t), \Delta_0, [\Delta])$ are ≥ 0 by (50)). The RHS is largest when $\underline{h}(q_A(t), [\Delta])$ is as negative as possible, so we examine this case.

First, want an upper bound on $\frac{-\alpha(\underline{h}(q_A(t), [\Delta]))}{\|r(t)\|} \frac{|r(t)_j|}{\|r(t)\|}$ (which occurs when $\underline{h}(q_A(t), [\Delta])$ is as negative as possible). Through the same line of reasoning as in (104) in App. A, $-\frac{1}{2}\sigma_M \|r(t)\|^2 + V_M \leq \underline{h}(q_A(t), [\Delta])$. Plugging in yields

$$\frac{-\alpha(\underline{h}(q_A(t), [\Delta]))}{\|r(t)\|} \frac{|r(t)_j|}{\|r(t)\|} \leq \frac{-\alpha(-\frac{1}{2}\sigma_M \|r(t)\|^2 + V_M)}{\|r(t)\|} \quad (108)$$

where we have used $|r(t)_j| \leq \|r(t)\|$. Using $\alpha(x) = \alpha_c x$, we have

$$\frac{-\alpha(-\frac{1}{2}\sigma_M \|r(t)\|^2 + V_M)}{\|r(t)\|} = \alpha_c \frac{1}{2}\sigma_M \|r(t)\| - \alpha_c \frac{V_M}{\|r(t)\|}. \quad (109)$$

The negative sign in front of V_M means that we want to divide by as large a value of $\|r(t)\|$ to make this negative quantity as small as possible to construct an upper bound. Recall that a bound on $\|r(t)\| \leq \varepsilon$ is already known from (54). With the uniform bound (51), this becomes

$$\alpha_c \frac{1}{2}\sigma_M \|r(t)\| - \alpha_c \frac{V_M}{\|r(t)\|} \leq \alpha_c \frac{1}{2}\sigma_M \varepsilon - \alpha_c \frac{V_M}{\varepsilon}. \quad (110)$$

Notice from (51) that $V_M = \frac{1}{2}\sigma_m \varepsilon^2$, and substituting gives

$$\frac{-\alpha(\underline{h}(q_A(t; k), [\Delta]))}{\|r(t)\|} \frac{|r(t; k)_j|}{\|r(t; k)\|} \leq \frac{\alpha_c \varepsilon (\sigma_M - \sigma_m)}{2}. \quad (111)$$

Next, we seek an upper bound on $\frac{|r(t)^\top w_M(q_A(t), \Delta_0, [\Delta])|}{\|r(t)\|} \frac{|r(t)_j|}{\|r(t)\|}$. With $w_M(\star)$ as in (84)

$$\frac{|r(t)^\top w_M(q_A(t), \Delta_0, [\Delta])|}{\|r(t)\|} \leq \frac{|r(t)^\top w_M(\star)|}{\|r(t)\|}. \quad (112)$$

where $w_M(\star) = w_M(\mathbf{q}_A(\mathbf{T}_i; \mathbf{K}), \Delta_0, [\Delta])$ for brevity. Bringing the norm of $w_M(\star)$ outside, we know that

$$\frac{|r(t)^\top w_M(\star)|}{\|r(t)\|} \frac{|r(t)_j|}{\|r(t)\|} = \|w_M(\star)\| \left(\frac{w_M(\star)^\top}{\|w_M(\star)\|} \frac{|r(t)|}{\|r(t)\|} \hat{z}_j^\top \frac{|r(t)|}{\|r(t)\|} \right), \quad (113)$$

where \hat{z}_j^\top is a unit vector comprised of all zeros except a 1 in the j^{th} dimension. The quantity in parentheses is a product of two dot products of unit vectors. Applying Lem. 23

$$\frac{|r(t)^\top w_M(q_A(t), \Delta_0, [\Delta])|}{\|r(t)\|} \frac{|r(t)_j|}{\|r(t)\|} \leq \frac{\|w_M(\star)\| + w_M(\star)_j}{2}. \quad (114)$$

Combine (111) and (114) with (107) to get the desired result. \square